Propofol Attenuates Lung but not Brain Cancer Cell Malignancy through Metabolism and Cell Signaling Modulation In Vitro

Cong Hu
Wenzhou Medical University Second Affiliated Hospital
Masae Iwasaki
Imperial College London
Zhigang Liu
Imperial College London
Bincheng Wang
Imperial College London
Xiaomeng Li
Imperial College London
Han Lin
Wenzhou Medical University Second Affiliated Hospital
Jun Li
Wenzhou Medical University Second Affiliated Hospital
Jia V. Li
Imperial College London
Qingquan Lian (wzmzlqq@163.com)
Wenzhou Medical University Second Affiliated Hospital
Daqing Ma (d.ma@imperial.ac.uk)
Imperial College London Faculty of Medicine https://orcid.org/0000-0002-0688-2097

Research

Keywords: Intravenous anesthetic, lung cancer, neuroglioma, metabolism, PEDF, HIF-1α

Posted Date: July 23rd, 2020

DOI: https://doi.org/10.21203/rs.3.rs-44983/v1

Propofol Attenuates Lung but not Brain Cancer Cell Malignancy through Metabolism and Cell Signaling Modulation *In Vitro*

Cong Hu[1,2], Masae Iwasaki[2,3], Zhigang Liu[4], Bincheng Wang[2], Xiaomeng Li[2], Han Lin[1], Jun Li[1], Jia V. Li[4], Qingquan Lian[1,*], Daqing Ma[2,*]

[1]Department of Anesthesiology, The Second Affiliated Hospital and Yuying Children's Hospital of Wenzhou Medical University, Wenzhou, Zhejiang, China

[2]Division of Anaesthetics, Pain Medicine and Intensive Care, Department of Surgery and Cancer, Faculty of Medicine, Imperial College London, Chelsea & Westminster Hospital, United Kingdom

[3]Department of Anesthesiology and Pain Medicine, Graduate School of Medicine, Nippon Medical School, Tokyo, Japan

[4]Department of Metabolism, Digestion and Reproduction, Faculty of Medicine, Imperial College London, United Kingdom

***Correspondence:** D Ma, Department of Surgery and Cancer, Faculty of Medicine, Imperial College London, Chelsea & Westminster Hospital, SW10 9NH, London, United Kingdom, Tel: +44 20 3315 8495, E-mail: d.ma@imperial.ac.uk

Or

QQ Lian, Department of Anesthesiology, The 2nd Affiliated Hospital and Yuying Children's Hospital of Wenzhou Medical University, 325027, Wenzhou, Zhejiang, P. R. China, Email: wzmzlqq@163.com

QL, JVL and DM share the senior authorship.

Abstract

Background: Intravenous anesthesia with propofol was reported to improve cancer surgical outcomes when compared with inhalational anesthesia. However, the underlying molecular mechanisms largely remain unknown. The current study aims to investigate whether propofol affects cancer cell biology including tumor metastasis-related gene expression, cellular signaling and metabolic changes in lung and brain cancer cells.

Methods: Lung cancer (A549) or neuroglioma (H4) cells were treated with propofol at a clinically relevant concentration (4 μg/mL) for 2 hours, followed by 24 hours recovery. Tumor metastasis-related gene expressions were assessed using a PCR array and validated with qRT-PCR. Glucose transporter 1 (GLUT1), brain protein 44-like (BRP44L), pigment epithelium-derived factor (PEDF), Akt, phospho-Akt (p-Akt), extracellular-signal-regulated kinase 1/2 (Erk1/2), phospho-Erk1/2 (p-Erk1/2), and hypoxia-inducible factor 1 alpha (HIF-1α) expressions were determined using immunofluorescent staining and/or western blotting. The metabolites in cell extract and media following propofol treatment were characterized using proton nuclear magnetic resonance (^{1}H NMR) spectroscopy. The malignant hallmarks including cell viability, proliferation, migration, and invasion were evaluated using cell counting kit-8 (CCK-8) assay, Ki-67 staining, wound healing and transwell assay, respectively.

Results: Propofol reduced cell viability and inhibited cell proliferation, migration and invasion of lung cancer cells, but not neuroglioma cells. In lung cancer cells, gene

expressions of *VEGFA, CTBP1, CST7, CTSK, CXCL12,* and *CXCR4* were downregulated, while *NR4A3, RB1, NME1, MTSS1, NME4, SYK, APC,* and *FAT1* were upregulated following the propofol treatment. Furthermore, propofol downregulated GLUT1, BRP44L, p-Akt, p-Erk, and HIF-1α expressions in lung cancer cells and upregulated PEDF expression. Propofol increased glutamate and glycine but decreased acetate and formate in lung cancer cells whilst increased lactate, valine, isoleucine, and leucine and glycerol, and decreased pyruvate and isopropanol in the culture media. Consistent with the phenotypical changes, these molecular and metabolic changes were not observed in the neuroglioma cells.

Conclusions: Our findings indicated “anti-tumor” effects of propofol on the lung cancer but not neuroglioma, through the regulation of tumor metastasis-related genes, multi-cellular signaling and cellular metabolism.

Keywords: Intravenous anesthetic; lung cancer; neuroglioma; metabolism; PEDF; HIF-1α.

Background

Cancer is the second leading disease of death worldwide (1, 2). Owing to ageing population globally, the incidence of cancer is increasing (2). Among all the types of cancers, lung cancer caused the highest mortality in adults reported in 2017 (3), whilst in children, the mortality of brain tumor is higher than other cancer types (4).

Surgery remains the primary therapy for solid organ cancer including lung cancer (5, 6). However, most cancer patients after surgery die due to the metastasis and recurrence. Recurrence can be the local, regional and distant recurrence (7) and the recurrence type, severity, and incidence are determined by many factors, including malignancy of cancer, surgical trauma and stress, adjuvant therapies and beyond (8).

It has been recognized that anesthetics and techniques may also contribute to the outcomes of cancer patients after surgery. For example, it was found that patients received inhalational anesthetics had a higher mortality rate when compared to those who were administered with intravenous anesthetic propofol during their surgical treatments for cancer (9). However, the mechanisms underlying these clinical observations remain unknown. A previous study demonstrated volatile anesthetics, such as, sevoflurane, isoflurane, and desflurane, upregulated the metastatic genes in ovarian cancer cells (10). Furthermore, unlike propofol, isoflurane was also demonstrated to increase hypoxia-inducible factor-1 alpha (HIF-1α) (11), which is a

transcriptional activator associated with the progression of a variety of cancer types, such as breast, colon, and lung cancer (12). HIF-1α can be activated by its upstream effectors, such as Akt and Erk1/2 (13, 14). Akt, also known as protein kinase B, belongs to the cAMP-dependent protein kinase superfamily, which is involved in many biological functions, for example, cell cycle, nutrient metabolism, and transcriptional regulation (15). Erk1/2 is also involved in a variety of biological functions, including proliferation, differentiation and cell survival (16). Akt and Erk1/2 signaling pathways can be regulated by a diversity of factors, such as pigment epithelium-derived factor (PEDF) (17, 18). PEDF is a secreted protein of serine protease inhibitor family and has anti-angiogenic, anti-tumor, and neurotrophic functions; and its therapeutic value for heart disease, choroidal neovascularization and cancer has been explored (19, 20).

In the current study, the role of PEDF and HIF-1α in anti-cancer property of propofol will be determined in lung and brain cancer cell cultures. We hypothesized that propofol downregulates glucose transporter 1 (GLUT1) and mitochondrial pyruvate carrier 1 (MPC1, also called BRP44L, brain protein 44-like) expressions, which leads to the disturbance of metabolisms of cancers. These changes may alter PEDF expression, which in turn, downregulates HIF-1α expression *via* Akt and Erk1/2 cellular signaling pathways. The suppression of HIF-1α expression finally affects tumor metastasis-related gene expressions and changes cancer cell malignancy and biology.

Methods

Cell culture

Lung cancer (A549) and neuroglioma (H4) cell lines were obtained from ECACC (Wiltshire, UK). A549 cell line was grown in Gibco RPMI media 1640 (ThermoFisher, Paisley, UK) supplemented with 10% fetal bovine serum (FBS) and 1% penicillin-streptomycin (ThermoFisher), while H4 cell line was cultured in Gibco Dulbecco's Modified Eagle Medium (ThermoFisher) supplemented with 10% FBS and 1% penicillin-streptomycin. A549 and H4 cells were cultured at 37ºC with 5% CO_2 and balanced with air. Cells were treated with 4 µg/mL propofol (Sigma-Aldrich, Dorset, UK) for 2 hours when the seeded cells formed a continuous monolayer. Intralipid (Santa Cruz Biotechnology, Dallas, Texas, USA) was used as vehicle control. After which, cell medium was replaced with fresh medium for the next 24 hours for further experiments.

Immunofluorescent staining

A549 and H4 cells were fixed with 4% paraformaldehyde solution in PBS (Santa Cruz Biotechnology) for 15 minutes, which was followed by the blocking procedure with 10% normal donkey serum (Sigma-Aldrich) for 30 minutes. After blocking, they were incubated with the primary antibodies (**Supplemental Table 1**) at 4ºC overnight and then probed with the secondary antibodies (**Supplemental Table 1**). The cells were mounted with DAPI (4', 6-diamidino-2-phenylindole) mounting media (Vector Laboratories, Burlingame, California, USA), and imaged by fluorescent microscopy.

ImageJ 2.0 software (National Institutes of Health, Bethesda, Maryland, USA) was used to quantify analysis wherever necessary.

Western blotting

Western blotting was done using our established protocol (10). The treated cells were lysed in cell lysis buffer (Cell Signaling, Danvers, Massachusetts, USA) and the protein concentration of the supernatant sample of cell lysis was measured. Protein samples with 60 µg were loaded into 4-12% polyacrylamide gel (Life Technologies, Paisley, UK) to be electrophoresed for 1.5 hour. After transferring the protein bands onto a PVDF membrane, the membrane was blocked with 5% non-fat milk for 1 hour, before incubation with the primary antibodies (**Supplemental Table 1**) at 4ºC overnight. After washing, the membrane was incubated with the secondary antibodies (**Supplemental Table 1**) for 1 hour at room temperature. The membrane was immersed with the enhanced chemiluminescence (ECL) system (Santa Cruz Biotechnology, Dallas, Texas, USA), and developed by GeneSnap (Syngene, Cambridge, UK). The intensity of blot bands was quantified with ImageJ 2.0.

Nuclear magnetic resonance spectroscopy

Cell pellets were placed into a bead beater tube (STARLAB Science Laboratory, Hamburg, Germany) containing 0.1 g sterile beads with a diameter of 0.1 mm and 1.5 mL of the pre-chilled mixture of methanol (Thermo Fisher) and water ($MeOH:H_2O$, v:v,

154 1:1). The tubes were placed in a bead beater (Bertin Instruments, Montigny-le-
155 Bretonneux, France) to homogenize the samples using two cycles of 6,500 Hz for 40
156 s with 5 min on dry ice between cycles. The samples were then centrifuged at 10,000
157 *g* at 4 °C for 10 min and the supernatants were transferred to new Eppendorf tubes
158 before drying at 45 ºC overnight and stored at -40 ºC. The dry cell extract samples
159 were resuspended in 210 µL of potassium phosphate buffer (pH=7.4) containing
160 deuterium oxide (D_2O) for magnetic field lock, 0.005% 3-(trimethylsilyl)-[2,2,3,3-$^2H_4$]-
161 propionic acid sodium salt (TSP) for the spectral calibration, 0.075 M KH_2PO_4, and 0.1
162 mM sodium azide (NaN_3). The resulting mixture was centrifuged at 20,817 *g* for 10 min,
163 and 180 µL supernatant was transferred to an NMR tube (Bruker Corporation,
164 Rheinstetten, Germany) with an outer diameter of 3 mm pending ^{1}H-NMR spectral
165 acquisition.
166
167 The cell media were thawed and centrifuged at 18,000 *g* for 10 min. A total of 540 µL
168 supernatant was mixed with 60 µL potassium phosphate buffer containing D_2O, 0.1%
169 TSP, 1.5 M KH_2PO_4 and 2 mM NaN_3. The mixture was transferred to an NMR tube with
170 an outer diameter of 5 mm pending ^{1}H NMR spectral acquisition.
171
172 The ^{1}H NMR spectra of cell extract and media samples were obtained using a Bruker
173 600 MHz spectrometer (Bruker Corporation, Rheinstetten, Germany) at the operating
174 ^{1}H frequency of 600.13 MHz at a temperature of 300 K. A standard NMR pulse

sequence (recycle delay-90º-t_1-90º-t_m-90º acquisition) was applied to acquire ^{1}H NMR spectral data (t_1 = 3 μs, t_m = 100 ms). The water peak suppression was achieved using selective irradiation during a recycle delay of 4 s and t_m. A 90º pulse was adjusted to ~10 μs. A total of 32 scans were collected into 64 k data points with a spectral width of 20 ppm.

PCR array

RNeasy mini kit® and QIAshredder (QIAGEN, West Sussex, UK) were employed to obtain total RNA from cells. A BioPhotometer (Eppendorf, Stevenage, UK) was used to determine the quantity and quality of RNA. The A260/A280 and A260/A230 ratio greater than 1.8 and 1.7 respectively, were regarded as sufficient quality for further analysis. The RT^2 First Strand Kit (QIAGEN) was utilized to convert total RNA to complementary DNA (cDNA), which was then mixed with SYBR Green ROX FAST Mastermix (QIAGEN). The mixture was added in an RT² Profiler™ PCR Array Human Tumor Metastasis (QIAGEN), which was processed and analyzed with the Rotor-Gene Q system (QIAGEN).

qRT-PCR

Paired oligonucleotide forward and reverse primers (**Supplemental Table 2**) for C-X-C motif chemokine 12 (*CXCL12*), C-X-C chemokine receptor type 4 (*CXCR4*), and GAPDH were designed using Primer Designer (Scientific and Educational Software,

196 Durham, USA) against the sequence downloaded from GenBank and obtained from
197 Invitrogen. The process of RNA extraction and cDNA generation was the same as
198 those in the PCR array experiment. The cDNA sample was mixed with forward and
199 reverse primers and SYBR Green ROX qPCR Mastermix (QIAGEN). The PCR mixture
200 was processed and analyzed with the Rotor-Gene Q system (QIAGEN). All mRNA data
201 were expressed relative to the endogenous control gene, GAPDH.
202
203 **Cell counting kit-8**
204 The cultured A549 and H4 cells were added with cell counting kit-8 (CCK-8) solution
205 (Sigma-Aldrich, Dorset, UK). The blank well is with media and cell counting kit-8
206 solution but without cells. Cancer cells were incubated at 37 ºC with 5% CO_2 for 2
207 hours. The optical density (OD) values were obtained *via* a microplate reader (BioTek,
208 Swindon, UK) at 450 nm wavelength. The cell viability value equals to (OD (Test) - OD
209 (Blank)) / (OD (Control) - OD (Blank)) X 100%.
210
211 **Wound healing scratch assay**
212 Cancer cells were scratched in the center of the confluent monolayer and taken a
213 picture under microscope as the baseline. The cells were incubated in medium without
214 FBS for 24 hours, after which the picture was taken again at the same site. The
215 percentage of scratching gap closure was analyzed with ImageJ 2.0.
216

Transwell assay

Cells were collected after the dissociation by trypsin (Sigma-Aldrich). They were re-suspended with serum-free media and seeded into the upper chamber of the transwell assay kit (Sigma-Aldrich), which was pre-embedded with Matrigel (Sigma-Aldrich) while the lower chamber was filled with serum-enrich media. After incubation for 24 hours, the upper chamber was fixed in 70% methanol for 30 minutes, which was followed by 15 minutes staining with 0.1% crystal violet (Sigma-Aldrich). After removal of the cells on the upper membrane, the cells remained on the bottom membrane were identified as invasive cells.

Statistical analysis

The data of western blotting, CCK-8, Ki-67 staining, wound healing assay, and transwell assay was analyzed by one-way analysis of variance (ANOVA) followed by Dunnett test for comparison (GraphPad Prism 8.2.0, GraphPad Software, La Jolla, California, USA). A two-sided p value of less than 0.05 was considered to be a statistical significance. The NMR data were imported and processed by MATLAB R2018a (MathWorks, Cambridge, UK) programming language with MATLAB scripts (21, 22). After data was normalized and aligned, principal component analysis (PCA) and orthogonal projections to latent structures discriminant analysis (OPLS-DA) were used to analyze the processed spectral data. The RNA array data was uploaded to GeneGlobe Data Analysis Centre (QIAGEN online program) and then analyzed.

Results

Effects of propofol on cancer malignancy in lung cancer and neuroglioma cells

Propofol decreased the cell viability of A549 cells (**Figure 1A**, NC *vs.* P, 100.00 ± 3.08 *vs.* 92.23 ± 1.83, $p < 0.0001$, $n = 8$), while there was no significant change in H4 cells (**Figure 1B**; NC *vs*. P, $p = 0.13$, $n = 8$). A significant decrease of Ki-67 positive cell numbers was observed in A549 cells treated with propofol compared with the naïve control (**Figure 1C** and **E,** NC *vs.* P, 32.73 ± 11.32 *vs.* 5.992 ± 1.019, $p < 0.01$, $n = 5$). In contrast, no change was detected in H4 cells (**Figure 1D** and **F**; $p = 0.44$ for NC *vs*. P, $n = 5$).

Propofol administration significantly decreased the migration of A549 cells (**Figure 2A** and **B**, NC *vs.* P, 53.84 ± 3.59 *vs.* 22.06 ± 4.71, $p < 0.001$, $n = 5$), but not H4 cells (**Figure 2C** and **D**; $p = 1.00$ for NC *vs*. P, $n = 5$). As shown by transwell assay, the invasion of A549 was significantly decreased (NC *vs.* P, 1.00 ± 0.14 *vs.* 0.67 ± 0.07, $p < 0.01$, $n = 5$) by propofol (**Figure 2E** and **F**), while no significant difference (NC *vs*. P, $p = 0.89$, $n = 5$) in numbers of invasive cells following propofol administration was seen in H4 cells (**Figure 2G** and **H**).

Propofol downregulated GLUT1 and BRP44L expressions in lung cancer cells but not in neuroglioma cells

The immunofluorescent staining of A549 cells showed GLUT1 (a cell membrane glucose transporter) and BRP44L (a mitochondrial pyruvate transporter) markers had clear co-expressions in naïve control group and vehicle control group, while both expressions in propofol group were significantly decreased (**Figure 3A**). The protein expressions of GLUT1 and BRP44L were significantly decreased in propofol group compared with naïve control group; the expression levels of GLUT1 (NC *vs.* P, 1.00 ± 0.69 *vs.* 0.29 ± 0.13, $p < 0.05$, $n = 6$) and BRP44L (NC *vs.* P, 1.00 ± 0.16 *vs.* 0.55 ± 0.09, $p < 0.01$, $n = 6$) (**Figure 3B-E**). In H4 cells, GLUT1 and BRP44L expressions had no changes among naïve control, vehicle control, and propofol groups in immunofluorescent staining (**Figure 4A, B**) and western blotting analysis (**Figure 4C-F**, NC *vs*. P, GLUT1, $p = 0.74$, BRP44L, $p = 0.99$, $n = 6$).

Propofol disturbed the metabolism of lung cancer cells but not neuroglioma cells

The ^{1}H NMR spectroscopy was used to analyze metabolite changes in cell extract and media samples of A549 and H4 cells. Pair-wise comparisons between control and propofol group of A549 and H4 cells were carried out using OPLS-DA analysis with one predictive component and one orthogonal component. R^2X, Q^2X, Q^2Y and permutation p values of OPLS-DA models were summarized in **Supplemental Table 3**. The changes of metabolites observed in pair-wise comparisons were shown in **Supplemental Table 4**. It showed a clear separation in A549 cell extracts between

control and propofol groups (**Figure 5A**). The significant difference was contributed by increased cellular concentrations of glutamate and glycine and decreased concentrations of formate and acetate in propofol group (**Figure 5B**). The separation in media samples between control and propofol groups of A549 cells was clearer than the cell extracts (**Figure 5C**). With propofol treatment, the concentrations of lactate, valine, isoleucine, leucine, glycerol and lipids were increased, while the concentrations of pyruvate and isopropanol were decreased (**Figure 5D**). However, no significant metabolic differences between the propofol and the control groups in either H4 cells or media (permutation p values > 0.05).

Propofol increased PEDF expressions in lung cancer cells but not in neuroglioma cells

PEDF expression in A549 and H4 cells was evaluated using immunofluorescent staining and western blotting. The immunofluorescent staining of A549 cells showed that the expression level of PEDF in propofol group was higher than naïve control group (**Figure 6A**). A significant increase in PEDF protein in the propofol group was observed compared with naïve control group based on western blotting analysis (NC *vs.* P, 1.00 ± 0.42 *vs.* 3.07 ± 1.95, $p < 0.05$, $n = 6$), but not between naïve and vehicle control groups in A549 cells (**Figure 6B** and **C**). The immunofluorescent staining (**Figure 6D**) and western blotting analysis (**Figure 6E** and **F**) of H4 cells showed no significant change between any groups analysis (NC *vs.* P, $p = 0.37$, $n = 6$).

Propofol suppressed both Akt and Erk pathways in lung cancer cells but not neuroglioma cells

Akt and Erk pathways, which could be affected by PEDF, were evaluated. The immunofluorescent staining showed both p-Akt (**Figure 7A**) and p-Erk (**Figure 7B**) of lung cancer cells were suppressed by propofol treatment. Western blotting analysis showed a significant decrease of p-Akt/Akt between naïve control and propofol group (NC *vs.* P, 1.00 ± 0.45 *vs.* 0.35 ± 0.07, $p < 0.01$, $n = 6$) (**Figure 7C** and **7D**). Moreover, the evaluation for p-Erk/Erk showed the similar pattern that a significant change was identified between naïve control and propofol group (NC *vs.* P, 1.00 ± 0.52 *vs.* 0.38 ± 0.07, $p < 0.01$, $n = 6$), but not between naïve and vehicle control group (**Figure 7E** and **F**). In H4 cells, there was no significant change between any groups of p-Akt/Akt (NC *vs*. P, $p = 1.00$, $n = 6$, **Figure 7G** and **7H**) and p-Erk/Erk (NC *vs*. P, $p = 0.72$, $n = 6$, **Figure 7I** and **7J**).

HIF-1α expression was downregulated by propofol in lung cancer cells but not neuroglioma cells

HIF-1α is one of the downstream pathways of Akt and Erk pathways. The immunofluorescent staining showed HIF-1α expression in A549 cells was decreased after propofol treatment (**Figure 8A**). HIF-1α expression in A549 cells measured by western blotting was also decreased in the propofol group (NC *vs.* P, 1.00 ± 0.20 *vs.*

0.67 ± 0.14, p < 0.01, n = 6) compared with naïve control group (**Figure 8B** and **C**). However, HIF-1α expression in H4 cells was not changed following propofol exposure (**Figure 8D, E** and **F**; p = 0.91 for NC vs. P of western blotting analysis, n = 6).

Effects of propofol on tumor metastatic related gene expressions of lung cancer and neuroglioma cells

Out of 84 tumor metastasis-related genes, 6 pro-tumor genes, namely, *VEGFA, CTBP1, CST7, CTSK, CXCL12, and CXCR4,* were downregulated in the propofol group compared with control. In addition, 8 anti-tumor genes including *NR4A3, RB1, NME1, MTSS1, NME4, SYK, APC, and FAT1* were upregulated (**Figure 9A**) in lung cancer cells. Among these altered gene expressions, *CXCL12* and *CXCR4* were significantly downregulated by propofol administration (**Figure 9B**, *CXCL12*, C *vs.* P, 1.000 ± 0.004 *vs.* 0.986 ± 0.004, p < 0.05, n = 3; **Figure 9C,** *CXCR4*, C *vs.* P, 1.000 ± 0.004 *vs.* 0.986 ± 0.004, p < 0.05, n = 3). These expression were subsequently validated by qRT-PCR, which showed consistent results with PCR array (**Figure 9D,** *CXCL12*, C *vs.* P, 1.00 ± 0.36 *vs.* 0.08 ± 0.04, p < 0.05, n = 3; **Figure 9E,** *CXCR4*, C *vs.* P, 1.00 ± 0.41 *vs.* 0.23 ± 0.16, p < 0.05, n = 3). However, there were no significant changes in *CXCL12* (**Figure 9F**, p = 0.35, n = 5) and *CXCR4* (**Figure 9G**, p = 0.79, n = 5) expressions in H4 cells between control and propofol groups.

Discussion

In the current study, we found that propofol, one of the most commonly used intravenous general anesthetic, downregulated GLUT1, BRP44L, HIF-1α, p-Akt and p-Erk1/2 expressions and upregulated PEDF in lung cancer cells but not in brain cancer cells (**Figure 10**). Furthermore, 6 pro-tumor genes were downregulated and 8 anti-tumor genes were upregulated after propofol administration, while the cell metabolism of lung cancer cells was altered by propofol. Ultimately, the cell viability, proliferation, migration and invasion of lung cancer cells were suppressed by propofol. However, these effects of propofol were not found in neuroglioma cells. Our data indicated that the malignancy of lung cancer cells was attenuated by propofol, which might be associate with the alterations of cell metabolisms and cell signaling pathways.

In this study, propofol was found to inhibit GLUT1 and BRP44L expressions, which were located at the cellular and mitochondrial membrane, respectively. In line with our data, propofol was previously reported to suppress GLUT1 expression in human myeloid leukemia cells (23). BRP44L, also known as mitochondrial pyruvate carrier 1, is responsible for transferring pyruvate into mitochondria for the tricarboxylic acid (TCA) cycle, which is a major energy synthesis pathway for normal cells (24). However, in contrast to normal cells, cancer cells are more likely to shift from mitochondrial oxidative phosphorylation to aerobic glycolysis, such phenomenon is called “Warburg effect” (25). “Warburg effect” requires the downregulation of BRP44L in cancer cells

364 and the BRP44L levels are relatively low in several cancer types, including lung cancer
365 (26, 27). Although cancer cells do not mainly rely on the TCA cycle to generate ATP, it
366 still requires the TCA cycle to produce the intermediates for the synthesis of nucleic
367 acids, fatty acids, and carbon skeleton (28). Interestingly, resveratrol is a phenolic
368 structured natural healthy supplement that not only blocks the activity of GLUT1, but
369 also downregulates the expression level of GLUT1. It was found that the exposure of
370 resveratrol to leukemic and ovarian cancer cells inhibits the uptake of glucose (29).
371 Resveratrol was found to inhibit the proliferation, metastasis and epigenetic alterations,
372 and induce the apoptosis *in vitro* and *in vivo* studies of breast cancer (30). Lonidamine,
373 an anti-tumor drug, was found to kill cancer cells by inhibiting the activity of BRP44L.
374 This was in agreement with our ^{1}H NMR spectral data, which showed that lactate in
375 the media of lung cancer cells was increased, while pyruvate was decreased by
376 propofol, indicating that pyruvate was more converted to lactate and less entered the
377 TCA cycle. This was very likely due to the decrease of BRP44L demonstrated in our
378 study while propofol itself induced mitochondrial bilayer perturbations might contribute
379 to this. In cancer cells, pyruvate is converted to formate and acetyl-CoA catalyzed by
380 pyruvate formate lyase, and acetyl-CoA can be metabolized to acetate or enter TCA
381 cycle (31). The concentrations of formate and acetate were decreased following the
382 administration of propofol, indicating pyruvate metabolism towards the production of
383 acetyl-CoA was reduced. In cancer cells, apart from glucose, glutamine is another
384 nutrition source, which is converted to glutamate and used in TCA cycle, namely

385 glutaminolysis (32). Our data showed that the concentration of glutamate was
386 increased in lung cancer cell extracts after treated with propofol, which was an
387 evidence of lower activity of glutaminolysis and TCA cycle. The metabolism of other
388 amino acids was also affected, including glycine, valine, isoleucine, and leucine.
389 Glycine was elevated in lung cancers administered with propofol. As glycine can be
390 converted to pyruvate, which is relevant with glucose metabolism or TCA cycle (33).
391 Isoleucine, leucine and valine was elevated in the media of propofol group, which
392 further indicted that propofol inhibited the metabolism of lung cancer cells, leading to
393 less utilization of amino acids. Isopropanol, a potential primary lung cancer biomarker
394 (34), was decreased in lung cancer cells with propofol treatment, suggesting that the
395 progression of lung cancer cells was inhibited by the treatment. Although the
396 metabolism of isopropanol was not fully understood, some reports claimed that
397 isopropanol might be transformed from acetone, which was converted from pyruvate
398 (35, 36). Another source of acetone is from beta-oxidation of fatty acids in mitochondria
399 (37). Propofol might injure mitochondrial beta-oxidation, which generated less acetone
400 to convert to isopropanol. These findings collectively indicated that propofol likely
401 causes mitochondrial injury and disturbs cancer cell metabolisms. It is true that
402 propofol is different from the other anesthetics as it has a unique phenolic structure,
403 which gives it a lipophilic property that can be solubilized inside the lipid membrane
404 bilayer and induce the lipid perturbations (38, 39), whilst the lipid bilayer is the platform
405 for protein-protein interaction and cellular signaling modulation, and its perturbations

406 can affect several signaling pathways and biochemical reactions (40).

407

408 It was reported that under high glucose concentration, PEDF expression was
409 decreased in retinal Muller cells (41, 42). In line with this, GLUT1 was downregulated
410 in lung cancer cells by propofol and less glucose uptake resulted in a relatively lower
411 concentration of glucose in cellular plasma of lung cancer cells. However, we did not
412 identify elevated glucose in media, which might due to other glucose transporters
413 (there is a total of 14 GLUTs expressed in human cells (43)) compensate the
414 decreased GLUT1 function. The compensation of GLUTs might cause a transient
415 change of glucose concentration in lung cancer cells that might induce the secretion
416 of PEDF, which was confirmed with our both immunofluorescent staining and western
417 blot data (**Figure 6**). PEDF has an anti-tumor and anti-angiogenesis property and
418 some tumor malignancy-related cellular signaling pathways in lung cancer cells may
419 likely be interrupted by the increased level of PEDF. Indeed, Akt and Erk in lung cancer
420 cells were inhibited by propofol as shown in our study and also reported previously (44,
421 45). Our group previously demonstrated that volatile anesthetic isoflurane enhanced
422 the malignancy of renal cancer cells by activating HIF-1α *via* Akt signaling pathway
423 (46). Overexpressed HIF-1α had been found in many aggressive cancer types and
424 was found to correlate with tumor progression (47, 48). In contrast to inhaled
425 anesthetics, propofol inactivated HIF-1α in lung cancer cells in the current study; this
426 is consistent with prostate cancer cells in which propofol inhibited the synthesis of HIF-

1α through Akt pathway which was initially induced by isoflurane and then suppressed by the superposition of propofol as we reported (11). HIF-1α is a key transcriptional regulator which are involved in cell survival, proliferation, migration and invasion (49). Our PCR array results showed that several pro-tumor (for example, *VEGFA, CXCL12*, and *CXCR4*) genes were downregulated and anti-tumor genes (for example, *RB1, APC,* and *FAT1*) were upregulated (Supplemental Table 5). These were in contrast to volatile anesthetics which induced the tumor metastatic related genes that were associated with the enhanced malignancy of ovarian cancer cells (10). Interestingly, a retrospective clinical study showed that patients received tumor resection were grouped into total intravenous anesthesia (propofol and remifentanil) or inhalational anesthesia (isoflurane or sevoflurane) groups. It was found that patients received inhalational anesthesia during cancer surgery had a lower 3 year-survival rate than those received propofol-based intravenous anesthesia (9). In another study, it was concluded that propofol-based intravenous anesthesia for colon cancer surgery was associated with better survival rate than desflurane-based inhalational anesthesia (50). Arguably, these clinical data are well supported by our current findings that propofol inhibits the malignancy of cancer cells, albeit derived from lung cancer.

In contrast, the expression of GLUT1, BRP44L, PEDF, p-Akt, p-Erk, and HIF-1α was not changed in neuroglioma cells by propofol. In addition, no significant changes were identified in our metabolism and PCR data. Unlike lung cancer cells, the cell viability,

448 proliferation, migration, and invasion of neuroglioma cells were not significantly
449 inhibited by propofol either. Why neuroglioma cells behaved so different to propofol
450 compared to lung cancer cells is unknown and warrants further study. One can argue
451 that, in general, brain cancer is very insensitive to chemotherapy and/or radiotherapy,
452 indicating that this type of cancer is more robust than other cancer types. Nevertheless,
453 our study may support clinical retrospective observations, in which patients were under
454 either propofol or sevoflurane maintenance of anesthesia for glioma resection and their
455 progression-free or overall survival were not different between two anesthetic
456 regimens (51, 52). The current study was based on *in vitro* assays and the future
457 investigation need to be carried out *in vivo* to evaluate the effect of propofol at the
458 systemic level. Clinically, there are many other risk factors, for example, surgery
459 induced inflammation and abnormal immune function during perioperative period, that
460 also affect the prognosis of cancer patients after surgery. It was reported that propofol
461 increased the cytotoxicity effects of natural killer (NK) cells, which might also benefit
462 the outcome of cancer patients (53). All these point to that propofol may be a good
463 choice of anesthetics used during surgery for certain cancer type but in order to better
464 simulate clinical scenarios, *in vivo* and clinical studies are required.
465
466 **Conclusions**
467 Our data suggested that unlike brain cancer cells, propofol disturbed the metabolism,
468 decreased GLUT1 and BRP44L expressions, and increased PEDF expression of lung

cancer cells. PEDF then inhibited HIF-1α *via* both Akt and Erk signaling and consequently upregulated anti-tumor genes and downregulated pro-tumor genes. The alteration of tumor metastatic related genes together with the disturbance of cellular metabolism may ultimately lead to the inhibition of malignancy of lung cancer cells. Our study could lead to new anesthetic regimens for cancer lung surgery. However, *in vitro* experimental setting cannot represent clinical scenario and, therefore, further clinical study/trial are required to valid the benefit effects of propofol found in our study.

List of Abbreviations

GLUT1: glucose transporter 1; BRP44L: brain protein 44-like; PEDF: pigment epithelium-derived factor; p-Akt: phospho-Akt; p-Erk: phospho-Erk; HIF-1α: hypoxia-inducible factor 1 alpha; ^{1}H NMR: proton nuclear magnetic resonance; CCK-8: cell counting kit-8; MPC1: mitochondrial pyruvate carrier 1; FBS: fetal bovine serum; 4', 6-diamidino-2-phenylindole: DAPI; ECL: enhanced chemiluminescence; D_2O: deuterium oxide; TSP: 3-(trimethylsilyl)-[2,2,3,3-$^{2}H_4$]-propionic acid sodium salt; NaN_3: sodium azide; cDNA: complementary DNA; CXCL12: C-X-C motif chemokine 12; CXCR4: C-X-C chemokine receptor type 4; OD: optical density; SD: standard deviation; ANOVA: one-way analysis of variance; PCA: principal component analysis; OPLS-DA: orthogonal projections to latent structures discriminant analysis; TCA: tricarboxylic acid; NK cell: natural killer cell.

Declarations

Ethics approval and consent to participate

Not applicable.

Consent for publication

Not applicable.

Availability of data and materials

The datasets used and/or analyzed during the current study are available from the corresponding author on reasonable request.

Completing interests

The authors declare that they have no completing interests.

Funding

CH was supported by a PhD scholarship (201700260043, 2017-2020) from China Scholarship Council, Beijing, China. JVL was funded by MRC New Investigator Grant (MR/P002536/1), MRC, London, UK and ERC Starting Grant (715662). DM was funded by BOC Chair grant, Royal College of Anaesthetists, London, UK. Partial research consumable cost was from the Second Affiliated Hospital and Yuying Children's Hospital of Wenzhou Medical University, Wenzhou, Zhejiang, China.

Author's contributions

DM, JVL, QL and CH designed the study. CH conducted cell culture, CCK-8, wound healing assay, Transwell assay, immunofluorescent staining, NMR sample extraction and preparation. CH and XL conducted double-stain immunofluorescence. CH and BW conducted Western blot. CH and ZL conducted NMR spectroscopic analysis. CH and MI conducted PCR array and qRT-PCR. CH and JVL conducted NMR data analysis. CH conducted other data analysis alone. CH drafted the manuscript. CH, MI, ZL, BW, XL, HL, JL, QL, JVL and DM participated in the review of the manuscript.

Acknowledgements

Figure 10 was created by using Servier Medical Art materials, which are licensed under a Creative Commons Attribution 3.0 Unported License.

References

1. Collaboration GBoDC. Global, Regional, and National Cancer Incidence, Mortality, Years of Life Lost, Years Lived With Disability, and Disability-Adjusted Life-years for 32 Cancer Groups, 1990 to 2015: A Systematic Analysis for the Global Burden of Disease Study. JAMA oncology. 2017;3(4):524-48.
2. Torre LA, Bray F, Siegel RL, Ferlay J, Lortet-Tieulent J, Jemal A. Global Cancer Statistics, 2012. Ca-a Cancer Journal for Clinicians. 2015;65(2):87-108.
3. Siegel RL, Miller KD, Jemal A. Cancer Statistics, 2017. Ca-a Cancer Journal for Clinicians. 2017;67(1):7-30.
4. A new clinical guideline from the Royal College of Paediatrics and Child Health with a national awareness campaign accelerates brain tumor diagnosis in UK children--"HeadSmart: Be Brain Tumour Aware". Neuro-oncology. 2016;18(3):445-54.

5. Aliperti LA, Predina JD, Vachani A, Singhal S. Local and systemic recurrence is the Achilles heel of cancer surgery. Annals of surgical oncology. 2011;18(3):603-7.
6. Ng JCH, See AAQ, Ang TY, Tan LYR, Ang BT, King NKK. Effects of surgery on neurocognitive function in patients with glioma: a meta-analysis of immediate post-operative and long-term follow-up neurocognitive outcomes. Journal of neuro-oncology. 2019;141(1):167-82.
7. Lee JS, Kim SI, Park HS, Lee JS, Park S, Park BW. The impact of local and regional recurrence on distant metastasis and survival in patients treated with breast conservation therapy. Journal of breast cancer. 2011;14(3):191-7.
8. Horowitz M, Neeman E, Sharon E, Ben-Eliyahu S. Exploiting the critical perioperative period to improve long-term cancer outcomes. Nature reviews Clinical oncology. 2015;12(4):213-26.
9. Wigmore TJ, Mohammed K, Jhanji S. Long-term Survival for Patients Undergoing Volatile versus IV Anesthesia for Cancer Surgery: A Retrospective Analysis. Anesthesiology. 2016;124(1):69-79.
10. Iwasaki M, Zhao H, Jaffer T, Unwith S, Benzonana L, Lian Q, et al. Volatile anaesthetics enhance the metastasis related cellular signalling including CXCR2 of ovarian cancer cells. Oncotarget. 2016;7(18):26042-56.
11. Huang H, Benzonana LL, Zhao H, Watts HR, Perry NJ, Bevan C, et al. Prostate cancer cell malignancy via modulation of HIF-1alpha pathway with isoflurane and propofol alone and in combination. British journal of cancer. 2014;111(7):1338-49.
12. Soni S, Padwad YS. HIF-1 in cancer therapy: two decade long story of a transcription factor. Acta oncologica (Stockholm, Sweden). 2017;56(4):503-15.
13. Jing Y, Liu LZ, Jiang Y, Zhu Y, Guo NL, Barnett J, et al. Cadmium increases HIF-1 and VEGF expression through ROS, ERK, and AKT signaling pathways and induces malignant transformation of human bronchial epithelial cells. Toxicological sciences : an official journal of the Society of Toxicology. 2012;125(1):10-9.
14. Wan J, Wu W. Hyperthermia induced HIF-1a expression of lung cancer through AKT and ERK signaling pathways. Journal of experimental & clinical cancer research : CR. 2016;35(1):119.
15. Mayer IA, Arteaga CL. The PI3K/AKT Pathway as a Target for Cancer Treatment. Annual review of medicine. 2016;67:11-28.
16. Samatar AA, Poulikakos PI. Targeting RAS-ERK signalling in cancer: promises and challenges. Nature reviews Drug discovery. 2014;13(12):928-42.
17. Yuan Y, Liu X, Miao H, Huang B, Liu Z, Chen J, et al. PEDF increases GLUT4-mediated glucose uptake in rat ischemic myocardium via PI3K/AKT pathway in a PEDFR-dependent manner. International journal of cardiology. 2019;283:136-43.
18. Sanchez A, Tripathy D, Yin X, Luo J, Martinez J, Grammas P. Pigment epithelium-derived factor (PEDF) protects cortical neurons in vitro from oxidant injury by activation of extracellular signal-regulated kinase (ERK) 1/2 and induction of Bcl-2. Neuroscience research. 2012;72(1):1-8.

19. Conte MI, Cabrillana ME, Saez Lancellotti TE, Simon L, Funes AK, Cayado-Gutierrez N, et al. Pigment epithelium derived factor (PEDF) expression in the male tract of Wistar rats. Biochem Biophys Res Commun. 2018;504(1):257-62.
20. Wei Y, Elahy M, Friedhuber AM, Wong JY, Hughes JD, Doschak MR, et al. Triple-threat activity of PEDF in bone tumors: Tumor inhibition, tissue preservation and cardioprotection against doxorubicin. Bone. 2019;124:103-17.
21. Trygg J, Holmes E, Lundstedt T. Chemometrics in metabonomics. J Proteome Res. 2007;6(2):469-79.
22. Haggart GA. csmsoftware/IMPaCTS: Version 1.1.1 (Version v1.1.1) Zenodo2019 [Available from: http://doi.org/10.5281/zenodo.3077413.
23. Tanaka T, Takabuchi S, Nishi K, Oda S, Wakamatsu T, Daijo H, et al. The intravenous anesthetic propofol inhibits lipopolysaccharide-induced hypoxia-inducible factor 1 activation and suppresses the glucose metabolism in macrophages. Journal of anesthesia. 2010;24(1):54-60.
24. Bricker DK, Taylor EB, Schell JC, Orsak T, Boutron A, Chen Y-C, et al. A mitochondrial pyruvate carrier required for pyruvate uptake in yeast, Drosophila, and humans. Science. 2012;337(6090):96-100.
25. Vander Heiden MG, Cantley LC, Thompson CB. Understanding the Warburg effect: the metabolic requirements of cell proliferation. science. 2009;324(5930):1029-33.
26. Lu Y, Yi Y, Liu P, Wen W, James M, Wang D, et al. Common human cancer genes discovered by integrated gene-expression analysis. PloS one. 2007;2(11):e1149-e.
27. Zou H, Chen Q, Zhang A, Wang S, Wu H, Yuan Y, et al. MPC1 deficiency accelerates lung adenocarcinoma progression through the STAT3 pathway. Cell death & disease. 2019;10(3):148-.
28. Anderson NM, Mucka P, Kern JG, Feng H. The emerging role and targetability of the TCA cycle in cancer metabolism. Protein Cell. 2018;9(2):216-37.
29. Zambrano A, Molt M, Uribe E, Salas M. Glut 1 in Cancer Cells and the Inhibitory Action of Resveratrol as A Potential Therapeutic Strategy. Int J Mol Sci. 2019;20(13).
30. Sinha D, Sarkar N, Biswas J, Bishayee A. Resveratrol for breast cancer prevention and therapy: Preclinical evidence and molecular mechanisms. Seminars in cancer biology. 2016;40-41:209-32.
31. Tack I, Nimmegeers P, Akkermans S, Logist F, Van Impe JFM. A low-complexity metabolic network model for the respiratory and fermentative metabolism of Escherichia coli. PloS one. 2018;13(8):e0202565.
32.Dang CV. Glutaminolysis: supplying carbon or nitrogen or both for cancer cells? Cell cycle (Georgetown, Tex). 2010;9(19):3884-6.
33. Cheng ZX, Guo C, Chen ZG, Yang TC, Zhang JY, Wang J, et al. Glycine, serine and threonine metabolism confounds efficacy of complement-mediated killing. Nature communications. 2019;10(1):3325.
34. Wehinger A, Schmid A, Mechtcheriakov S, Ledochowski M, Grabmer C, Gastl

622 GA, et al. Lung cancer detection by proton transfer reaction mass-spectrometric
623 analysis of human breath gas. International Journal of Mass Spectrometry.
624 2007;265(1):49-59.
625 35. Lewis GD, Laufman AK, McAnalley BH, Garriott JC. Metabolism of acetone to
626 isopropyl alcohol in rats and humans. J Forensic Sci. 1984;29(2):541-9.
627 36. Li WW, Liu Y, Liu Y, Cheng SQ, Duan YX. Exhaled isopropanol: new potential
628 biomarker in diabetic breathomics and its metabolic correlations with acetone.
629 Rsc Advances. 2017;7(28):17480-8.
630 37. Laffel L. Ketone bodies: a review of physiology, pathophysiology and
631 application of monitoring to diabetes. Diabetes Metab Res Rev. 1999;15(6):412-
632 26.
633 38. Reitz M, Velizarov S, Glück B, Berg H, Brambrink AM. Effects of propofol
634 (intravenous propofol emulsion) on cell membrane measures by electrofusion and
635 electroporation. Arzneimittel-Forschung/Drug Research. 1999;49(3):281-5.
636 39. Bahri MA, Seret A, Hans P, Piette J, Deby-Dupont G, Hoebeke M. Does propofol
637 alter membrane fluidity at clinically relevant concentrations? An ESR spin label
638 study. Biophysical Chemistry. 2007;129(1):82-91.
639 40. Hicks DA, Nalivaeva NN, Turner AJ. Lipid rafts and Alzheimer's disease:
640 protein-lipid interactions and perturbation of signaling. Frontiers in physiology.
641 2012;3:189.
642 41. Mu H, Zhang X-M, Liu J-J, Dong L, Feng Z-L. Effect of high glucose concentration
643 on VEGF and PEDF expression in cultured retinal Müller cells. Molecular biology
644 reports. 2009;36(8):2147.
645 42. Yamagishi S-i, Matsui T. Pigment epithelium-derived factor (PEDF) and
646 cardiometabolic disorders. Current pharmaceutical design. 2014;20(14):2377-86.
647 43. Thorens B, Mueckler M. Glucose transporters in the 21st Century. American
648 journal of physiology Endocrinology and metabolism. 2010;298(2):E141-5.
649 44. Hsing C-H, Lin M-C, Choi P-C, Huang W-C, Kai J-I, Tsai C-C, et al. Anesthetic
650 propofol reduces endotoxic inflammation by inhibiting reactive oxygen species-
651 regulated Akt/IKKβ/NF-κB signaling. PloS one. 2011;6(3):e17598.
652 45. Fibuch EE, Wang JQ. Inhibition of the MAPK/ERK cascade: a potential
653 transcription-dependent mechanism for the amnesic effect of anesthetic propofol.
654 Neuroscience bulletin. 2007;23(2):119-24.
655 46. Benzonana LL, Perry NJ, Watts HR, Yang B, Perry IA, Coombes C, et al.
656 Isoflurane, a commonly used volatile anesthetic, enhances renal cancer growth
657 and malignant potential via the hypoxia-inducible factor cellular signaling
658 pathway in vitro. Anesthesiology. 2013;119(3):593-605.
659 47. Unwith S, Zhao H, Hennah L, Ma D. The potential role of HIF on tumour
660 progression and dissemination. International journal of cancer Journal
661 international du cancer. 2015;136(11):2491-503.
662 48. Zhao H, Iwasaki M, Yang J, Savage S, Ma D. Hypoxia-inducible factor-1: a
663 possible link between inhalational anesthetics and tumor progression? Acta

anaesthesiologica Taiwanica : official journal of the Taiwan Society of Anesthesiologists. 2014;52(2):70-6.
49. Semenza GL. Targeting HIF-1 for cancer therapy. Nature reviews Cancer. 2003;3(10):721-32.
50. Wu ZF, Lee MS, Wong CS, Lu CH, Huang YS, Lin KT, et al. Propofol-based Total Intravenous Anesthesia Is Associated with Better Survival Than Desflurane Anesthesia in Colon Cancer Surgery. Anesthesiology. 2018;129(5):932-41.
51. Dong J, Zeng M, Ji N, Hao S, Zhou Y, Gao Z, et al. Impact of Anesthesia on Long-term Outcomes in Patients With Supratentorial High-grade Glioma Undergoing Tumor Resection: A Retrospective Cohort Study. Journal of neurosurgical anesthesiology. 2020;32(3):227-33.
52. Saito J, Masters J, Hirota K, Ma D. Anesthesia and brain tumor surgery: technical considerations based on current research evidence. Current opinion in anaesthesiology. 2019;32(5):553-62.
53. Li R, Liu H, Dilger JP, Lin J. Effect of Propofol on breast Cancer cell, the immune system, and patient outcome. BMC anesthesiology. 2018;18(1):77.

693 **Figure legends**

694 **Figure 1. The cell viability and proliferative capability of lung cancer and**
695 **neuroglioma cells after propofol exposure.**

696 Lung cancer A549 and neuroglioma H4 cells were treated with intralipid (vehicle
697 control), 4 μg/mL propofol, or pure culture media (naïve control). Cell viability of lung
698 cancer (**A**) and neuroglioma cells (**B**) was evaluated with the CCK-8 assay. Cell
699 proliferative capability of A549 (**C**) and H4 cells (**D**) with Ki-67 immunofluorescent
700 staining. The comparison of Ki-67 positive cell percentage in A549 cells (**E**) and H4
701 cells (**F**). Data were expressed as mean ± standard deviation and dot plot (n = 5-8).
702 **p < 0.01, ****p < 0.0001 versus naïve control. Scale bar: 100 μm. NC, naïve control;
703 VC, vehicle control; P, propofol.

704

705 **Figure 2. The migrate and invasive ability of lung cancer and neuroglioma cells**
706 **after propofol administration.**

707 Lung cancer A549 and neuroglioma H4 cells were administered with intralipid (vehicle
708 control), 4 μg/mL propofol, or no treatment (naïve control). The migration of lung cancer
709 (**A**) and neuroglioma cells (**C**) was assessed *via* wound healing assay with statistical
710 analysis of the percentage of gap closure of A549 (**B**) and H4 cells (**D**). The invasion
711 of A549 (**E**) and H4 cells (**G**) was evaluated by Transwell assay with the statistical
712 analysis of the relative ratio of invasive cell number to NC in A549 (**F**) and H4 cells (**H**).
713 Data were presented as mean ± standard deviation and dot plot (n = 5). **p < 0.01,

714 ***p < 0.001 versus naïve control. Scale bar: 100 μm. NC: naïve control; V: vehicle
715 control; P: propofol.
716
717 **Figure 3. Propofol down-regulated GLUT1 and BRP44L in lung cancer cells.**
718 Lung cancer A549 cells were administered with 4 μg/mL propofol or intralipid (vehicle
719 control) or media without drugs (naïve control) for 2 hours followed by 24 hours
720 recovery time. GLUT1 (green) and BRP44L (red) expressions were identified by dual-
721 immunofluorescent staining (**A**). The expression levels of GLUT1 (**B** and **C**) and
722 BRP44L (**D** and **E**) were validated with western blotting analysis. The intensity of
723 western blotting bands was normalized by housekeeping gene GAPDH. Data were
724 analyzed with one-way analysis of variance (ANOVA) followed by Dunnett multi-
725 comparison test. Data were presented as mean ± standard deviation and dot plot (n =
726 6). *p < 0.05; **p < 0.01 versus naïve control. Scale bar: 50 μm. NC: naïve control; VC:
727 vehicle control; P: propofol; GLUT1: glucose transporter 1; BRP44L: brain protein 44-
728 like.
729
730 **Figure 4. GLUT1 and BRP44L expressions in neuroglioma cells after**
731 **administered with propofol.**
732 Neuroglioma H4 cells were administered with a clinically relevant concentration of 4
733 μg/mL propofol. GLUT1 (green) and BRP44L (red) expressions were analyzed by
734 immunofluorescent staining (**A** and **B**) and validated with western blotting (**C-F**). The

735 intensity of Western blot bands was normalized by housekeeping gene GAPDH. Data
736 were analyzed with one-way analysis of variance (ANOVA) followed by Dunnett multi-
737 comparison test. Data were presented as mean ± standard deviation and dot plot (n =
738 6). Scale bar: 50 μm. NC: naïve control; VC: vehicle control; P: propofol; GLUT1:
739 glucose transporter 1; BRP44L: brain protein 44-like.
740
741 **Figure 5. The metabolism alterations of lung cancer cells after propofol**
742 **administration.**
743 Orthogonal projection to latent structures-discriminant analysis (OPLS-DA) loadings
744 plots from ^{1}H NMR spectral data of the A549 cell extract (**A** and **B**) and A549 media
745 samples (**C** and **D**) for comparisons as control *vs.* propofol (n = 9-10). **A** and **C**: OPLS-
746 DA scores plot; **B** and **D**: OPLS-DA loadings plot. The color bar indicates the
747 correlation coefficient values (r^2) to be high in red and low in blue. C: control; P:
748 propofol; F: formate; Glu: glutamate; Gly: glycine; Ace: acetate; Lac: lactate; Gro:
749 glycerol; Pyr: pyruvate; FA: fatty acids; IPA: isopropanol; Val: valine; Ile: isoleucine;
750 Leu: leucine.
751
752 **Figure 6. Propofol up-regulated PEDF in lung cancer cells but not neuroglioma**
753 **cells.**
754 Lung cancer A549 and neuroglioma H4 cells were administered with a clinically
755 relevant concentration 4 μg/mL of propofol for 2 hours. PEDF expression was analyzed

by immunofluorescent staining (**A.** A549 cells and **D**. H4 cells) and western blotting analysis (**B.** A549 cells and **E.** H4 cells). PEDF (green) was overlaid with DAPI (blue). The intensity of western blotting bands was normalized by housekeeping gene GAPDH (**C**. A549 cells and **F**. A549 cells). Data were analyzed with one-way analysis of variance (ANOVA) followed by Dunnett multi-comparison test. Data were presented as mean ± standard deviation and dot plot (n = 6). *p < 0.05 versus naïve control. Scale bar: 50 μm. NC, naïve control; VC, vehicle control; P, propofol; PEDF; pigment epithelium-derived factor.

Figure 7. Propofol down-regulated Akt and Erk expression in lung cancer cells but not neuroglioma cells.

Lung cancer A549 and neuroglioma H4 cells were treated with 4 μg/mL propofol or vehicle control or naïve control. **A**. p-Akt (green) of lung cancer cells as cytoplasmic dyeing overlaid with DAPI (blue) staining in nucleus. **B**. p-Erk1/2 (green) was stained in cytoplasm overlaid with DAPI (blue) in the nucleus. **C**. The representative western blotting bands of p-Akt and Akt expression of A549 cells. **D**. The relative ratio of p-Akt to Akt compared to naïve control of A549 cells. **E**. The representative bands of p-Erk1/2 and Erk1/2 expression of A549 cells. **F.** The representative western blotting bands of p- Erk1/2 and Erk1/2 expression of A549 cells. **G.** The representative bands of p-Akt and Akt expression of H4 cells. **H.** The relative ratio of p-Akt to Akt compared to naïve control of H4 cells. **I.** The representative bands of p-Erk1/2 and Erk1/2 expression of

H4 cells. **J.** The representative western blotting bands of p-Erk1/2 and Erk1/2 expression of H4 cells. Data were analyzed with one-way analysis of variance (ANOVA) followed by Dunnett multi-comparison test. Data were presented as mean ± standard deviation and dot plot (n = 6). **p < 0.01 versus naïve control. Scale bar: 50 μm. NC: naïve control; VC: vehicle control; P: propofol; p-Akt: phospho-Akt; Erk1/2: extracellular-signal-regulated kinase 1/2; p-Erk1/2: phospho-Erk 1/2.

Figure 8. HIF-1α expression in lung cancer and neuroglioma cells after propofol administration.

The immunofluorescent staining with the dye of HIF-1α (green) co-stained with DAPI (blue) for lung cancer A549 cells (**A**) and neuroglioma H4 cells (**D**). The representative western blotting bands of HIF-1α and GAPDH of lung cancer (**B**) and neuroglioma (**E**). The statistical analysis of the relative ratio of HIF-1α to GAPDH in A549 cells (**C**) and H4 cells (**F**). Data were analyzed with one-way analysis of variance (ANOVA) followed by Dunnett multi-comparison test. Data were presented as mean ± standard deviation and dot plot (n = 6). **p < 0.01 versus naïve control. Scale bar: 50 μm. NC, naïve control; VC, vehicle control; P, propofol, HIF-1α: hypoxia-inducible factor-1 alpha.

Figure 9. Propofol alters lung cancer cell mRNA expression levels of tumor metastatic related genes assessed by PCR array and qRT-PCR.

Lung cancer A549 and neuroglioma H4 cells were treated with 4 μg/mL propofol or

798 intralipid as the control for 2 hours and then recovered for up to 24 hours. **A**. The PCR
799 array analysis of tumor metastatic related genes. Unsupervised hierarchical cluster
800 analysis using Euclidean distance from the low-density arrays. Propofol up-regulated
801 8 anti-tumor genes and down-regulated 6 pro-tumor genes of A549 cells (n = 3). The
802 data is relative to endogenous control, GAPDH. Red and green colors indicate
803 relatively high and low expression, respectively. The results of *CXCL12* (**B**) and
804 *CXCR4* (**C**) obtained from A549 cells using PCR array and qRT-PCR (**D**: CXCL12 and
805 **E**: CXCR4, n = 3). The expression levels of *CXCL12* gene (**F**) and *CXCR4* gene (**G**)
806 from H4 cells evaluated with qRT-PCR (n = 5). Data were expressed as mean ±
807 standard deviation and dot plot. *p < 0.05 versus control. C: control; P: propofol;
808 VEGFA: vascular endothelial growth factor A; CTBP1: C-terminal binding protein 1;
809 CST7: cystain 7; CTSK: cathepsin K; CXCL12: C-X-C motif chemokine 12; CXCR4:
810 C-X-C chemokine receptor type 4; NR4A3: nuclear receptor subfamily 4 group A
811 member 3; RB1: retinoblastoma susceptility 1; NME1: NME/NM23 nucleoside
812 diphosphate kinase 1; MTSS1: metastasis suppressor I-BAR domain containing 1;
813 NME4: NME/NM23 nucleoside diphosphate kinase 4; SYK: spleen tyrosine kinase;
814 APC: adenomatous polyposis coli; FAT1: FAT tumor suppressor homolog 1.
815
816 **Figure 10. The cellular signaling interactions in lung cancer cells after propofol**
817 **administration.**
818 Propofol down-regulates GLUT1, which decreases glucose uptake into cell plasma.

Propofol also down-regulates BRP44L expression, which converts pyruvate more to lactate and less to formate and acetate or enters TCA cycle. The decreased level of TCA activity inhibits the generation of intermediates for the synthesis of nucleic acids, fatty acids, and carbon skeleton. The Lower intracellular glucose concentration induces the secretion of PEDF. PEDF inhibits both Akt and Erk phosphorylation, which leads to the downregulation of HIF-1α. HIF-1α is translocated into the nucleus and acts as a key transcriptional regulator to increase anti-tumor-related genes or decrease pro-tumor-related genes. Propofol disturbs metabolism and alters tumor metastatic related and ultimately inhibits the malignancy of lung cancer cells.

GLUT1: glucose transporter 1; BRP44L: brain protein 44-like; TCA: tricarboxylic acid; PEDF: pigment epithelium-derived factor; Erk1/2: extracellular signal-regulated kinase 1/2; HIF-1α: hypoxia-inducible factor 1 alpha.

Figures

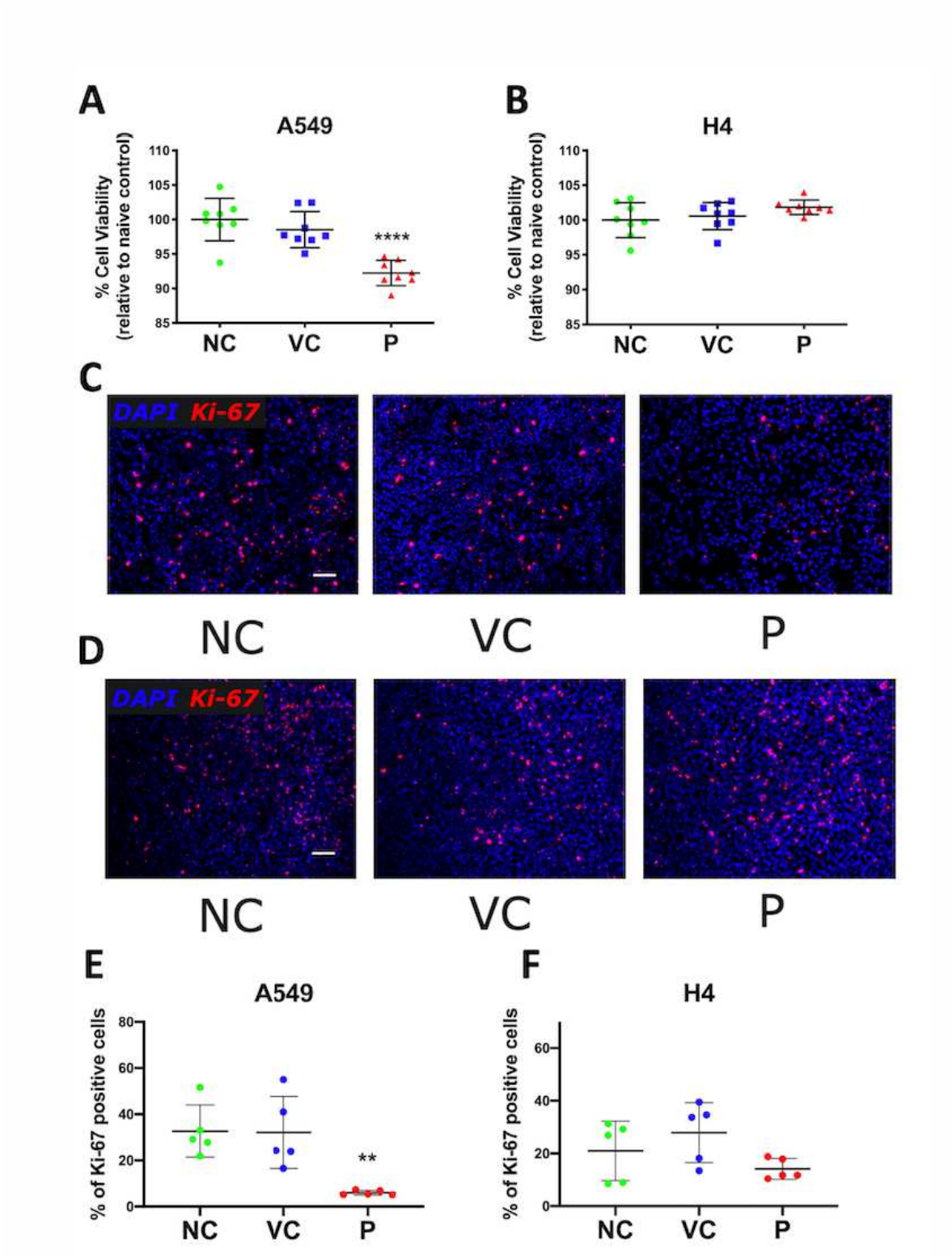

Figure 1

The cell viability and proliferative capability of lung cancer and neuroglioma cells after propofol exposure. Lung cancer A549 and neuroglioma H4 cells were treated with intralipid (vehicle control), 4 μg/mL propofol, or pure culture media (naïve control). Cell viability of lung cancer (A) and neuroglioma

cells (B) was evaluated with the CCK-8 assay. Cell proliferative capability of A549 (C) and H4 cells (D) with Ki-67 immunofluorescent staining. The comparison of Ki-67 positive cell percentage in A549 cells (E) and H4 cells (F). Data were expressed as mean ± standard deviation and dot plot (n = 5-8). **p < 0.01, ****p < 0.0001 versus naïve control. Scale bar: 100 μm. NC, naïve control; VC, vehicle control; P, propofol.

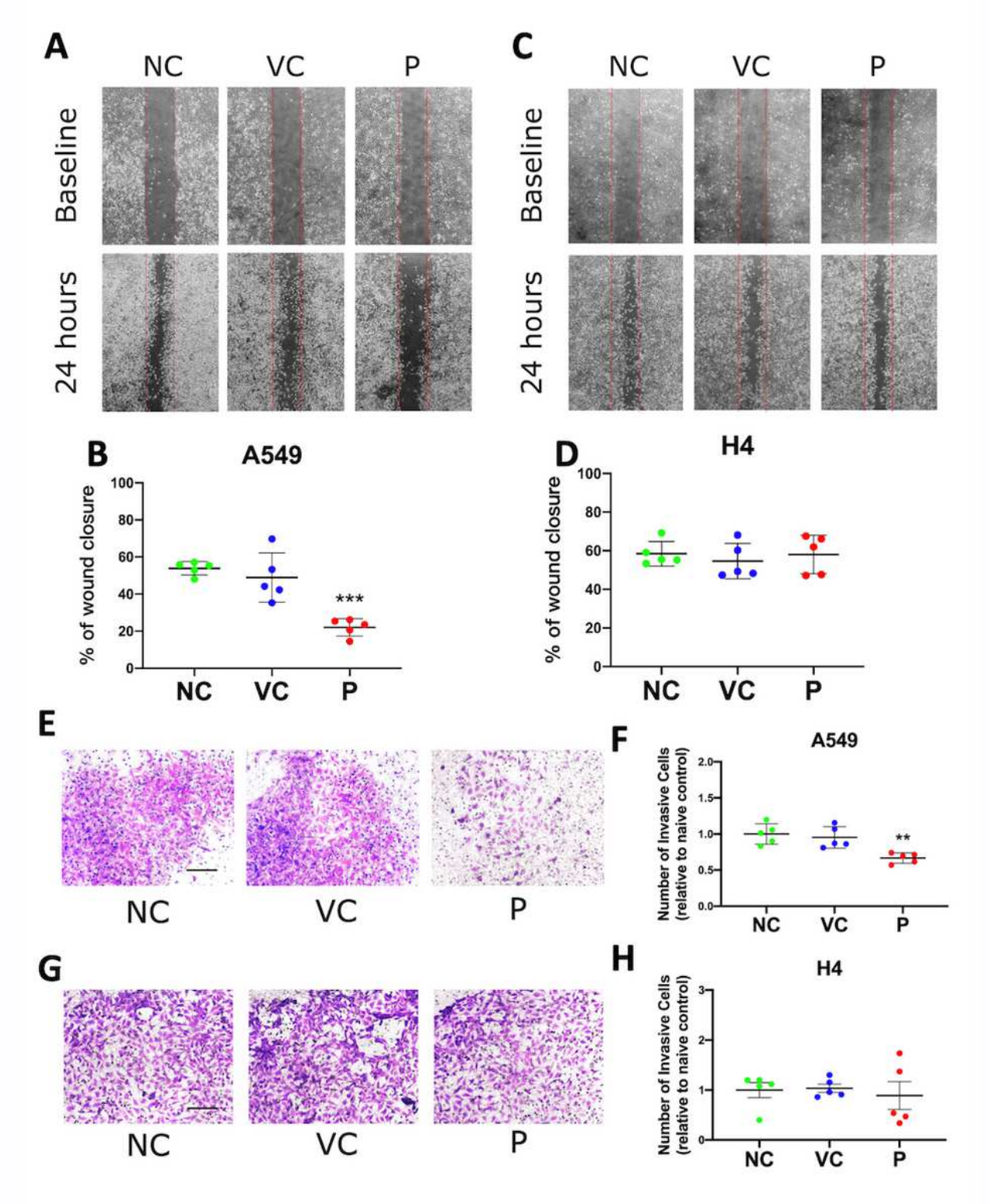

Figure 2

The migrate and invasive ability of lung cancer and neuroglioma cells after propofol administration. Lung cancer A549 and neuroglioma H4 cells were administered with intralipid (vehicle control), 4 μg/mL propofol, or no treatment (naïve control). The migration of lung cancer (A) and neuroglioma cells (C) was assessed via wound healing assay with statistical analysis of the percentage of gap closure of A549 (B) and H4 cells (D). The invasion of A549 (E) and H4 cells (G) was evaluated by Transwell assay with the statistical analysis of the relative ratio of invasive cell number to NC in A549 (F) and H4 cells (H). Data were presented as mean ± standard deviation and dot plot (n = 5). **p < 0.01, ***p < 0.001 versus naïve control. Scale bar: 100 μm. NC: naïve control; V: vehicle control; P: propofol.

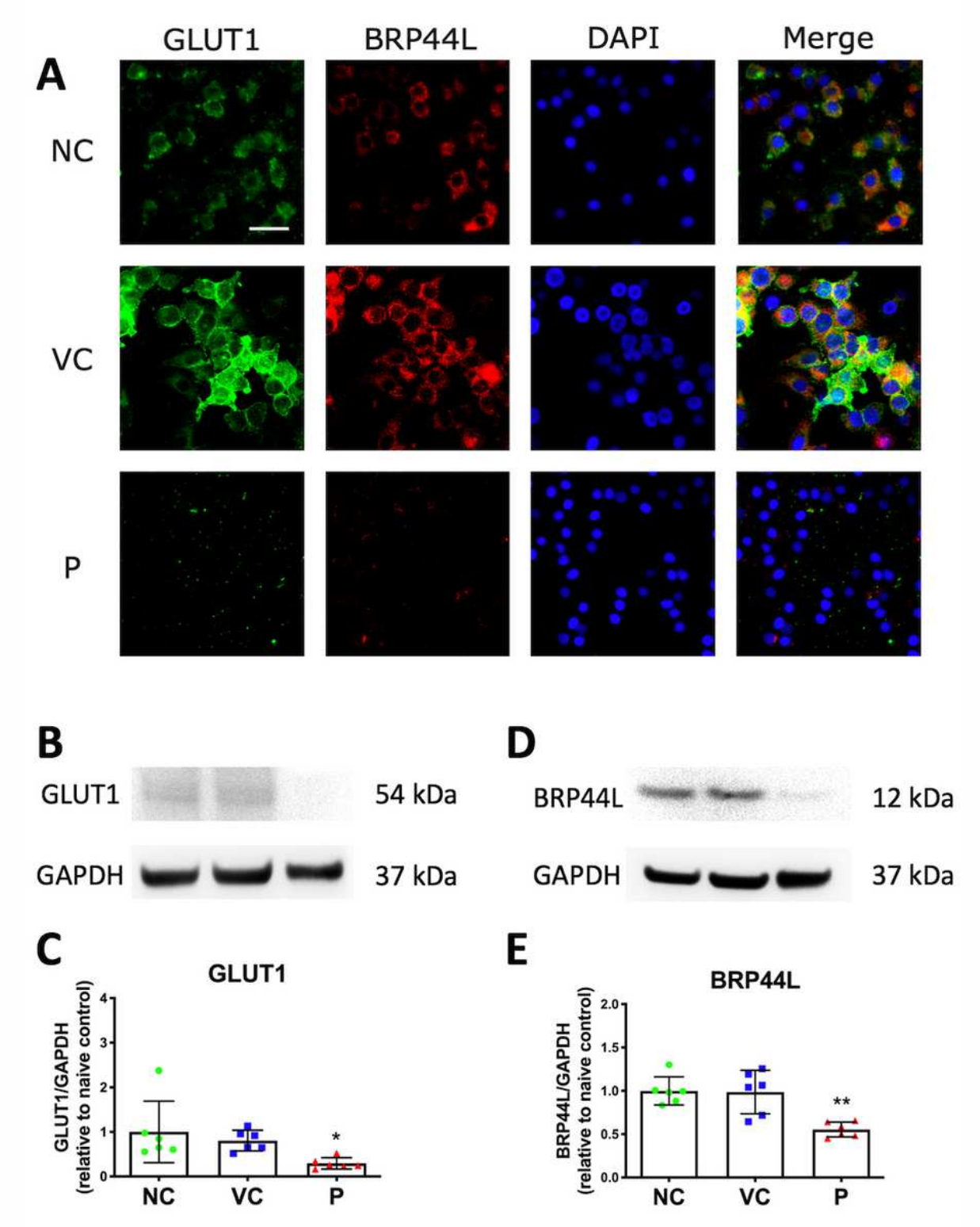

Figure 3

Propofol down-regulated GLUT1 and BRP44L in lung cancer cells. Lung cancer A549 cells were administered with 4 μg/mL propofol or intralipid (vehicle control) or media without drugs (naïve control) for 2 hours followed by 24 hours recovery time. GLUT1 (green) and BRP44L (red) expressions were identified by dual-immunofluorescent staining (A). The expression levels of GLUT1 (B and C) and BRP44L (D and E) were validated with western blotting analysis. The intensity of western blotting bands was

normalized by housekeeping gene GAPDH. Data were analyzed with one-way analysis of variance (ANOVA) followed by Dunnett multi-comparison test. Data were presented as mean ± standard deviation and dot plot (n = 6). *p < 0.05; **p < 0.01 versus naïve control. Scale bar: 50 μm. NC: naïve control; VC: vehicle control; P: propofol; GLUT1: glucose transporter 1; BRP44L: brain protein 44- like.

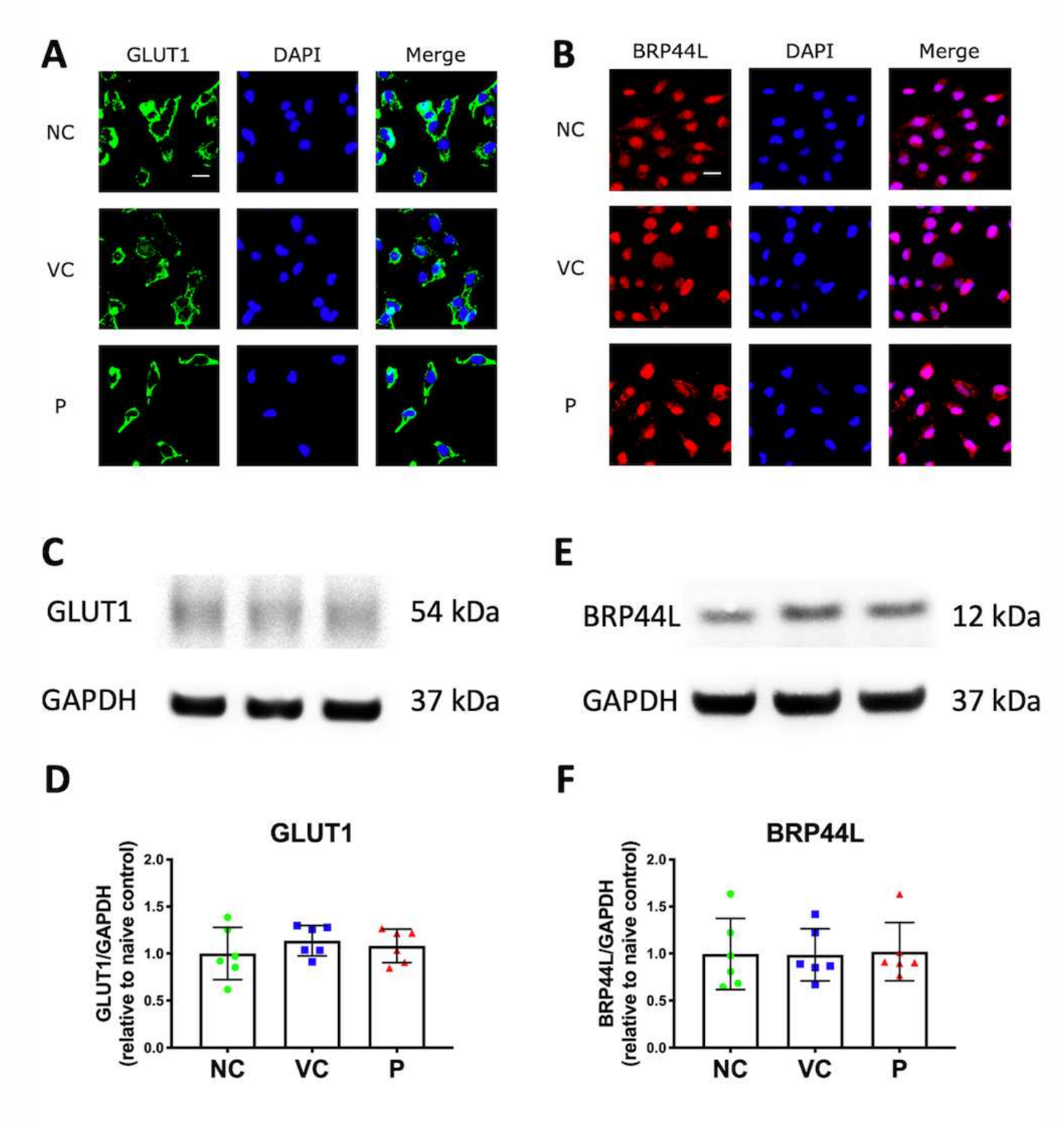

Figure 4

GLUT1 and BRP44L expressions in neuroglioma cells after administered with propofol. Neuroglioma H4 cells were administered with a clinically relevant concentration of 4 μg/mL propofol. GLUT1 (green) and BRP44L (red) expressions were analyzed by immunofluorescent staining (A and B) and validated with western blotting (C-F). The intensity of Western blot bands was normalized by housekeeping gene GAPDH. Data were analyzed with one-way analysis of variance (ANOVA) followed by Dunnett multicomparison test. Data were presented as mean ± standard deviation and dot plot (n = 6). Scale bar: 50 μm. NC: naïve control; VC: vehicle control; P: propofol; GLUT1: glucose transporter 1; BRP44L: brain protein 44-like.

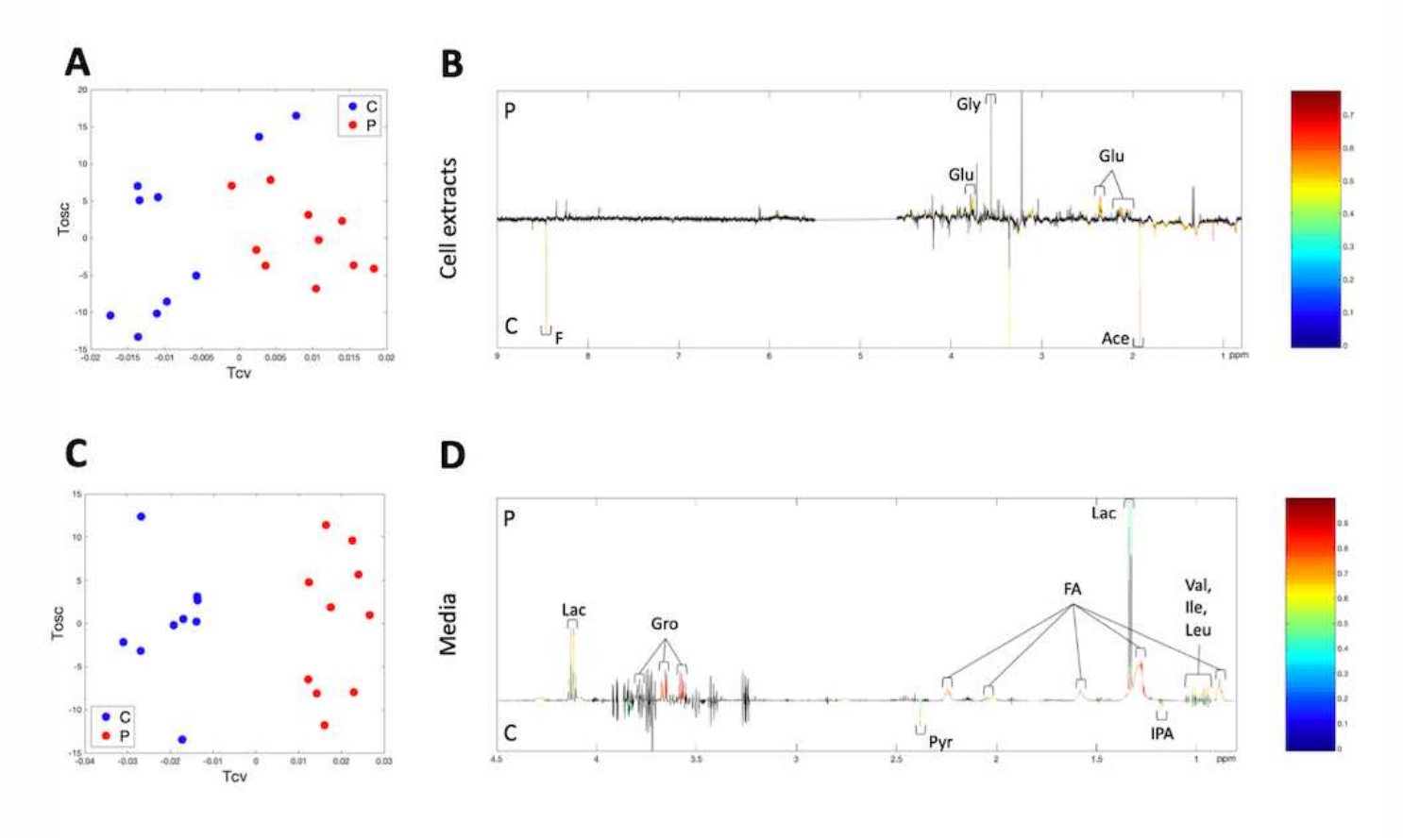

Figure 5

The metabolism alterations of lung cancer cells after propofol administration. Orthogonal projection to latent structures-discriminant analysis (OPLS-DA) loadings plots from 1H NMR spectral data of the A549 cell extract (A and B) and A549 media samples (C and D) for comparisons as control vs. propofol (n = 9-10). A and C: OPLSDA scores plot; B and D: OPLS-DA loadings plot. The color bar indicates the correlation coefficient values (r2) to be high in red and low in blue. C: control; P: propofol; F: formate; Glu: glutamate; Gly: glycine; Ace: acetate; Lac: lactate; Gro: glycerol; Pyr: pyruvate; FA: fatty acids; IPA: isopropanol; Val: valine; Ile: isoleucine; Leu: leucine.

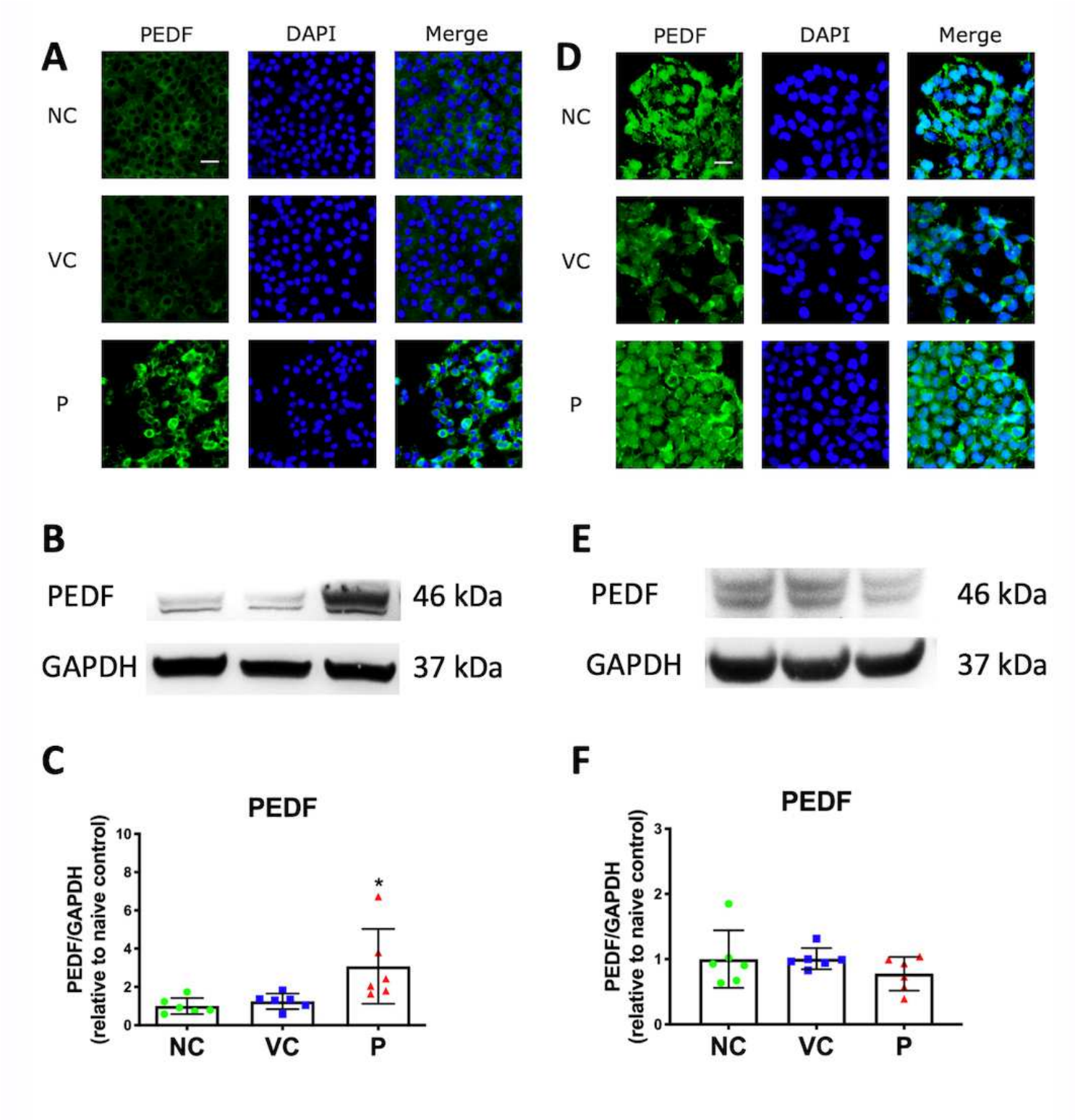

Figure 6

Propofol up-regulated PEDF in lung cancer cells but not neuroglioma cells. Lung cancer A549 and neuroglioma H4 cells were administered with a clinically relevant concentration 4 μg/mL of propofol for 2 hours. PEDF expression was analyzed by immunofluorescent staining (A. A549 cells and D. H4 cells) and western blotting analysis (B. A549 cells and E. H4 cells). PEDF (green) was overlaid with DAPI (blue). The intensity of western blotting bands was normalized by housekeeping gene GAPDH (C. A549 cells and F.

A549 cells). Data were analyzed with one-way analysis of variance (ANOVA) followed by Dunnett multi-comparison test. Data were presented as mean ± standard deviation and dot plot (n = 6). *p < 0.05 versus naïve control. Scale bar: 50 μm. NC, naïve control; VC, vehicle control; P, propofol; PEDF; pigment epithelium-derived factor.

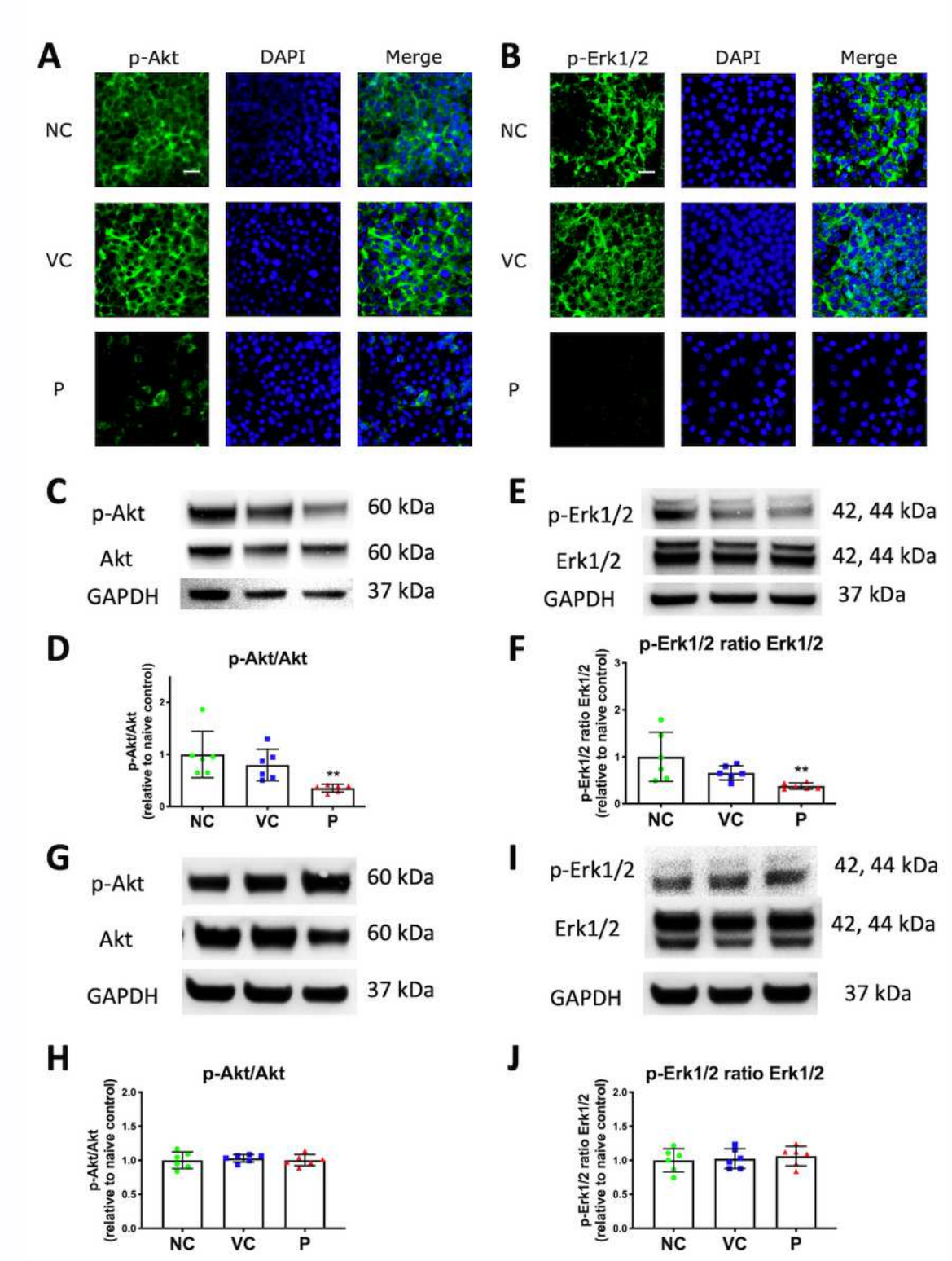

Figure 7

Propofol down-regulated Akt and Erk expression in lung cancer cells but not neuroglioma cells. Lung cancer A549 and neuroglioma H4 cells were treated with 4 μg/mL propofol or vehicle control or naïve control. A. p-Akt (green) of lung cancer cells as cytoplasmic dyeing overlaid with DAPI (blue) staining in nucleus. B. p-Erk1/2 (green) was stained in cytoplasm overlaid with DAPI (blue) in the nucleus. C. The representative western blotting bands of p-Akt and Akt expression of A549 cells. D. The relative ratio of p-Akt to Akt compared to naïve control of A549 cells. E. The representative bands of p-Erk1/2 and Erk1/2 expression of A549 cells. F. The representative western blotting bands of p- Erk1/2 and Erk1/2 expression of A549 cells. G. The representative bands of p-Akt and Akt expression of H4 cells. H. The relative ratio of p-Akt to Akt compared to naïve control of H4 cells. I. The representative bands of p-Erk1/2 and Erk1/2 expression of H4 cells. J. The representative western blotting bands of p-Erk1/2 and Erk1/2 expression of H4 cells. Data were analyzed with one-way analysis of variance (ANOVA) followed by Dunnett multi-comparison test. Data were presented as mean ± standard deviation and dot plot (n = 6). **$p < 0.01$ versus naïve control. Scale bar: 50 μm. NC: naïve control; VC: vehicle control; P: propofol; p-Akt: phospho-Akt; Erk1/2: extracellular-signal-regulated kinase 1/2; p-Erk1/2: phospho-Erk 1/2.

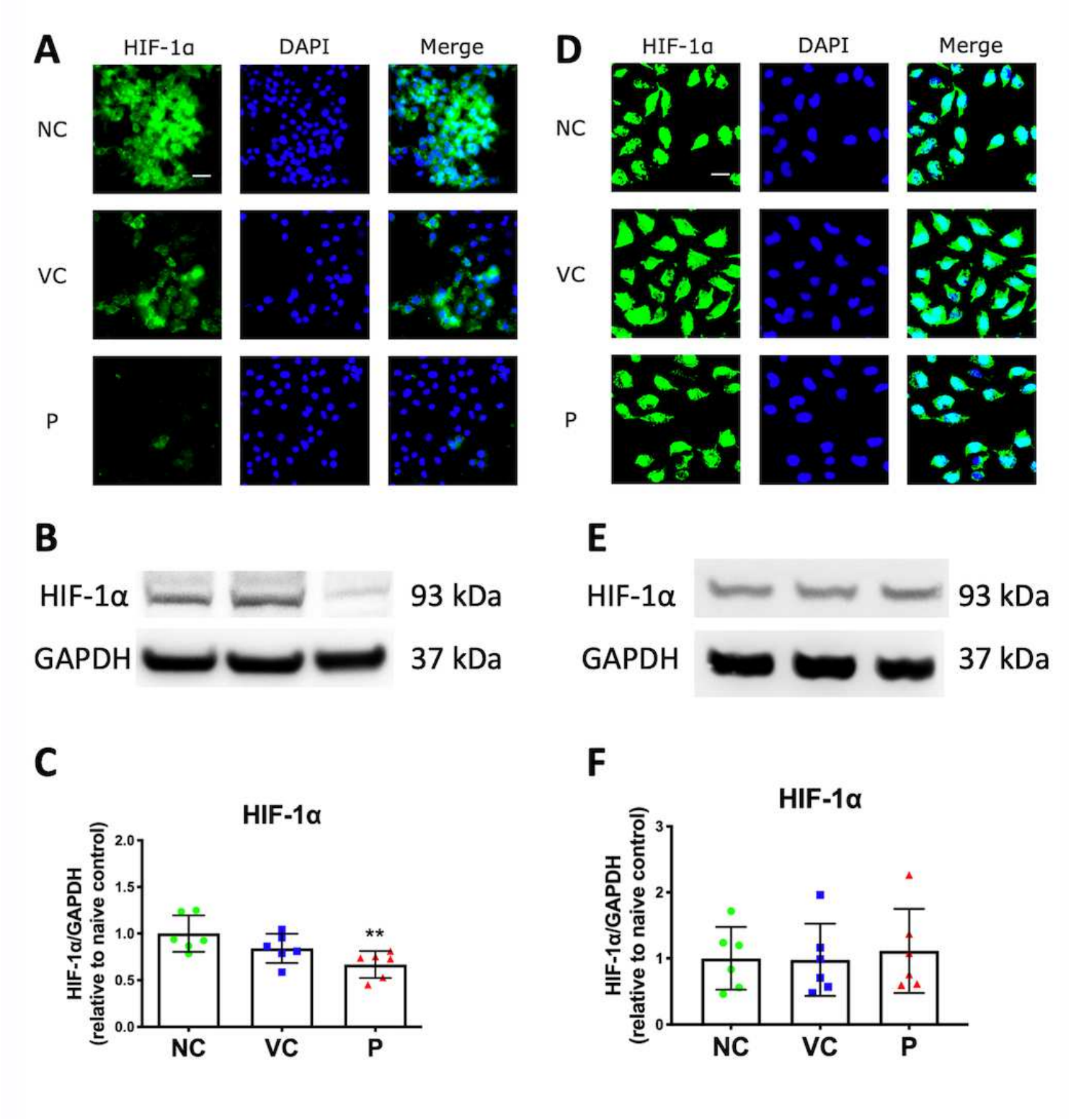

Figure 8

HIF-1α expression in lung cancer and neuroglioma cells after propofol administration. The immunofluorescent staining with the dye of HIF-1α (green) co-stained with DAPI (blue) for lung cancer A549 cells (A) and neuroglioma H4 cells (D). The representative western blotting bands of HIF-1α and GAPDH of lung cancer (B) and neuroglioma (E). The statistical analysis of the relative ratio of HIF-1α to GAPDH in A549 cells (C) and H4 cells (F). Data were analyzed with one-way analysis of variance

(ANOVA) followed by Dunnett multi-comparison test. Data were presented as mean ± standard deviation and dot plot (n = 6). **p < 0.01 versus naïve control. Scale bar: 50 μm. NC, naïve control; VC, vehicle control; P, propofol, HIF-1α: hypoxia-inducible factor-1 alpha.

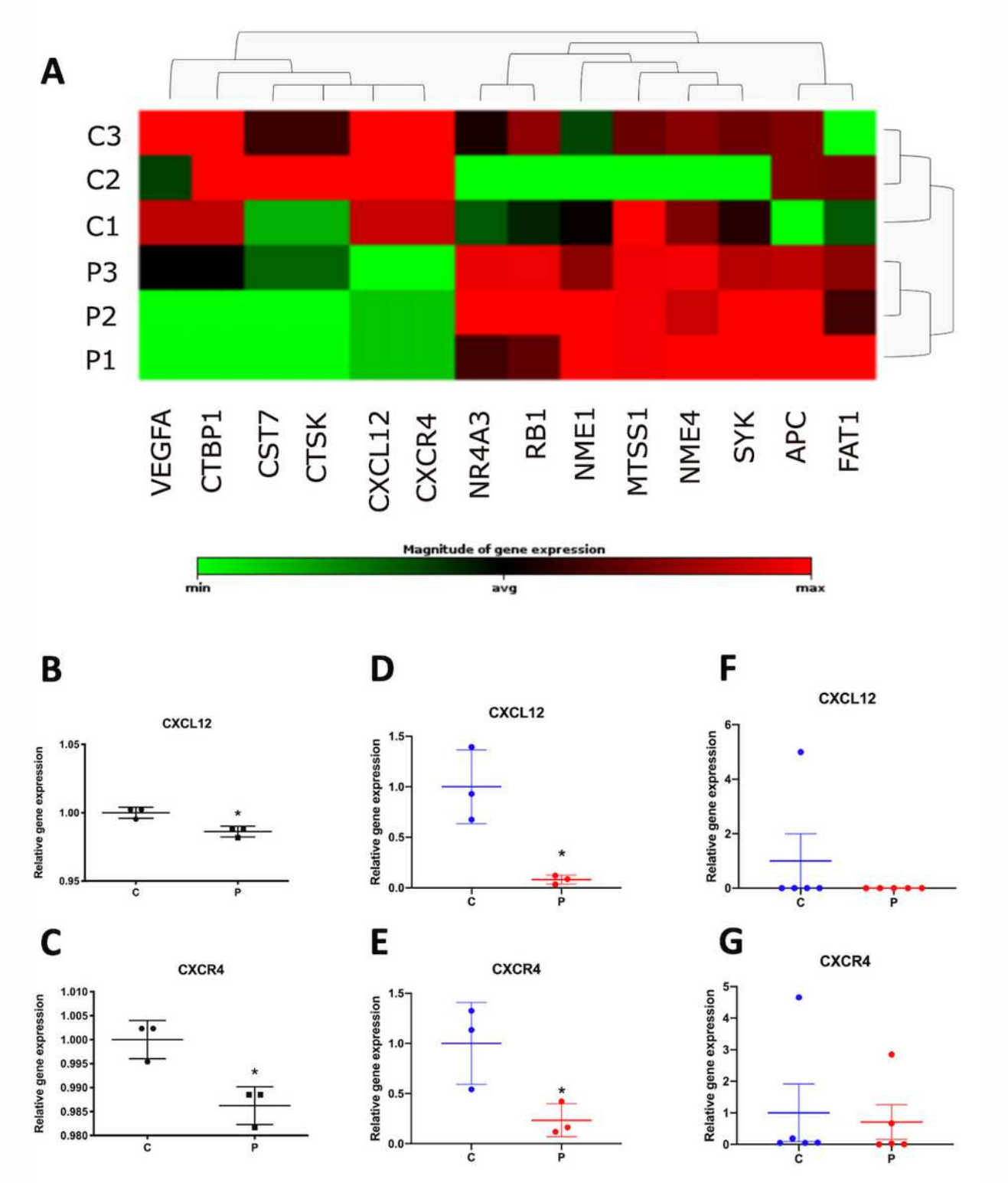

Figure 9

Propofol alters lung cancer cell mRNA expression levels of tumor metastatic related genes assessed by PCR array and qRT-PCR. Lung cancer A549 and neuroglioma H4 cells were treated with 4 μg/mL propofol

or intralipid as the control for 2 hours and then recovered for up to 24 hours. A. The PCR array analysis of tumor metastatic related genes. Unsupervised hierarchical cluster analysis using Euclidean distance from the low-density arrays. Propofol up-regulated 8 anti-tumor genes and down-regulated 6 pro-tumor genes of A549 cells (n = 3). The data is relative to endogenous control, GAPDH. Red and green colors indicate relatively high and low expression, respectively. The results of CXCL12 (B) and CXCR4 (C) obtained from A549 cells using PCR array and qRT-PCR (D: CXCL12 and E: CXCR4, n = 3). The expression levels of CXCL12 gene (F) and CXCR4 gene (G) from H4 cells evaluated with qRT-PCR (n = 5). Data were expressed as mean ± standard deviation and dot plot. *$p < 0.05$ versus control. C: control; P: propofol; VEGFA: vascular endothelial growth factor A; CTBP1: C-terminal binding protein 1; CST7: cystain 7; CTSK: cathepsin K; CXCL12: C-X-C motif chemokine 12; CXCR4: C-X-C chemokine receptor type 4; NR4A3: nuclear receptor subfamily 4 group A member 3; RB1: retinoblastoma susceptility 1; NME1: NME/NM23 nucleoside diphosphate kinase 1; MTSS1: metastasis suppressor I-BAR domain containing 1; NME4: NME/NM23 nucleoside diphosphate kinase 4; SYK: spleen tyrosine kinase; APC: adenomatous polyposis coli; FAT1: FAT tumor suppressor homolog 1.

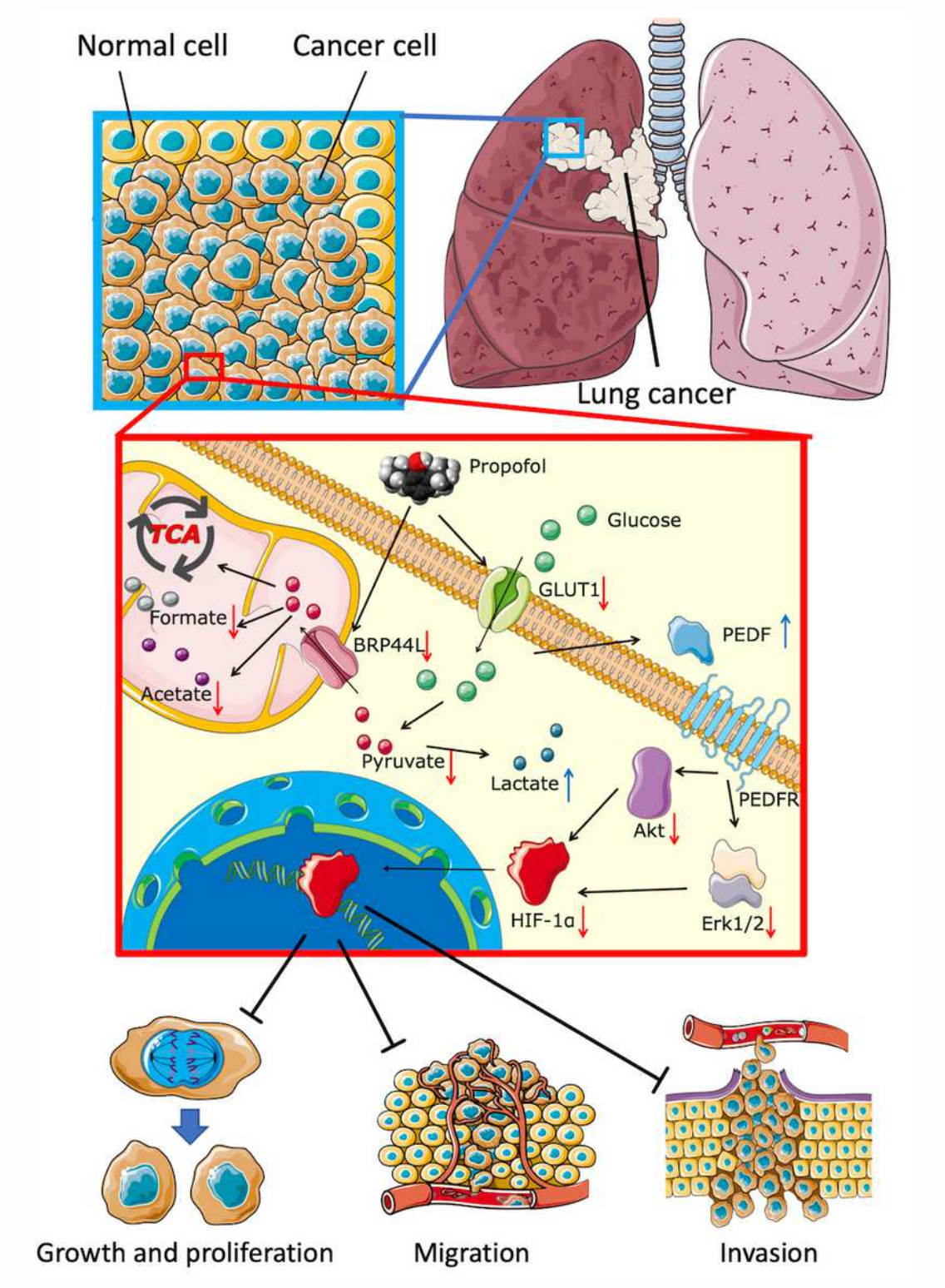

Figure 10

The cellular signaling interactions in lung cancer cells after propofol administration. Propofol down-regulates GLUT1, which decreases glucose uptake into cell plasma. Propofol also down-regulates BRP44L expression, which converts pyruvate more to lactate and less to formate and acetate or enters TCA cycle. The decreased level of TCA activity inhibits the generation of intermediates for the synthesis of nucleic acids, fatty acids, and carbon skeleton. The Lower intracellular glucose concentration induces

the secretion of PEDF. PEDF inhibits both Akt and Erk phosphorylation, which leads to the downregulation of HIF-1α. HIF-1α is translocated into the nucleus and acts as a key transcriptional regulator to increase anti-tumor-related genes or decrease protumor- related genes. Propofol disturbs metabolism and alters tumor metastatic related and ultimately inhibits the malignancy of lung cancer cells. GLUT1: glucose transporter 1; BRP44L: brain protein 44-like; TCA: tricarboxylic acid; PEDF: pigment epithelium-derived factor; Erk1/2: extracellular signal-regulated kinase 1/2; HIF-1α: hypoxia-inducible factor 1 alpha.

Supplementary Files

This is a list of supplementary files associated with this preprint. Click to download.

- Supplements.docx
- Supplements.docx